Relatório de Atividades de 2001 da Linha de Pesquisa e Desenvolvimento em Fusão Termonuclear Controlada – FUSÃO
Laboratório Associado de Plasma – LAP

Descrição

O objetivo geral desta linha é pesquisar plasmas em confinamento magnético, através do desenvolvimento de tokamaks esféricos e sistemas auxiliares de diagnóstico e aquecimento de plasma, visando a geração futura de energia por fusão. Mais especificamente, os objetivos são:

- Investigar sistemas toroidais compactos de confinamento magnético de plasma, acompanhando os avanços internacionais na área.
- Desenvolver o tokamak esférico ETE, explorando as propriedades desta configuração e seu potencial como um reator a fusão de geometria compacta, alto beta e operação contínua.
- Desenvolver sistemas de aquecimento de plasma e geração de corrente, notadamente por injeção de ondas de radiofreqüência, e sistemas de diagnóstico de plasma de alta temperatura adequados aos tokamaks esféricos.

Pessoal envolvido

- **Equipe Permanente e Atribuições**

  Dr. Edson Del Bosco (Operação da máquina, Diagnósticos, Chefe do LAP – Tempo parcial)
  Dr. Gerson Otto Ludwig (Responsável pela linha de pesquisa, Teoria e Engenharia)
  Dr. Joaquim José Barroso de Castro (Fontes de microondas – Tempo parcial)
  Dr. Luiz Ângelo Berni (Diagnósticos)
  Dra. Maria Célia Ramos de Andrade (Teoria)
  Dr. Pedro José de Castro (Medidas eletromagnéticas – Tempo parcial)
  Ms. Carlos Shinya Shibata (Tratamento de dados – Tempo parcial)
  Ms. Heitor Patire Júnior (Desenvolvimento do monotron)
  Ms. Júlio Guimarães Ferreira (Fontes de potência, Diagnósticos)
  Ms. Rogério de Moraes Oliveira (Controle e aquisição de dados, Diagnósticos)
  Alice Hitomi Nakahara Ueda (Técnica Química)
  Francisco Eugênio Donatelli de Figueiredo Costa (Técnico Eletrônico – Tempo parcial)
  David Carlos de Jesus (Auxiliar Técnico)
  Jorge Weber Santana do Nascimento (Auxiliar Técnico)
  Márcia Veiga Vicente de Moraes (Secretária do LAP – Tempo parcial)

- **Equipe Temporária**

  Dr. Konstantin Gueorguiev Kostov (Simulação numérica do monotron)
  Bolsista FAPESP/Pesquisador Visitante de 09/09/2000 a 08/09/2001
  Ms. Luis Filipe de Faria Pereira Wiltgem Barbosa (Sistema de controle por redes neurais)
  Bolsista FAPESP/Doutorado ITA a partir de 01/10/1998
  Waldeir Amaral Vilela (Engenheiro Eletrônico – Bancos de capacitores e medidas elétricas)
  Bolsista DTI MCT/PCI a partir de 01/01/1998
  Alberto Barbosa da Silva (Técnico Mecânico – Fabricação de peças)
  Bolsista DTI MCT/PCI a partir de 01/05/1997
  Artur Faria de Oliveira (Técnico Mecânico – Fabricação de peças)
  Bolsista DTI MCT/PCI a partir de 01/04/2000
  Carlos Alberto Maia Jr. (Técnico Mecânico – Fabricação de peças para diagnósticos)
  Bolsista FAPESP de 01/09/1999 a 30/03/2001
  Marco Antonio Marcondes de Abreu Marques (Técnico Mecânico – Desenvolvimento e fabricação de peças)
  Bolsista DTI MCT/PCI de 01/07/2000 a 31/05/2001

Marcos Fiorio Gama Lobo (Técnico Eletrônico – Bancos de capacitores e sistema de vácuo)
Bolsista DTI MCT/PCI de 01/05/1997 a 31/05/2001
Néliton Gonçalves de Oliveira (Técnico em Informática – Interfaces dos sistemas de controle e aquisição de dados)
Bolsista DTI MCT/PCI de 01/12/2000 a 31/05/2001

Resultados

O desenvolvimento experimental em anos anteriores pode ser resumido da seguinte forma. A fabricação de componentes do ETE foi iniciada em meados de 1995 e quase inteiramente realizada no Laboratório Associado de Plasma do INPE, com recursos financeiros e humanos extremamente limitados. A montagem do ETE começou em junho de 1998 após completada a construção do novo laboratório. Uma precisão melhor que 2 mm foi obtida na montagem conforme especificações detalhadas e restritivas de projeto. Testes da máquina tiveram início em novembro de 1999, envolvendo os sistemas auxiliares de aquecimento da câmara de vácuo e de limpeza por descarga luminescente, enquanto procedia a montagem dos bancos de capacitores. O primeiro plasma de tokamak no ETE foi obtido em 28 de novembro de 2000 com hidrogênio à pressão de $2{,}4\times10^{4}$ mbar. A corrente de plasma atingiu 11,6 kA e a duração do pulso 1,2 ms.

A campanha de 2001 teve como objetivo melhorar as condições de vácuo e de formação do plasma. Realizou-se um estudo da ruptura de gases injetados no ETE em três condições de pré-ionização: sem pré-ionização, utilizando luz ultravioleta, e utilizando um chuveiro de elétrons produzidos por emissão termoiônica. Os campos magnéticos de êrro, que têm um papel importante durante as fases de ruptura do gás e formação do plasma, foram medidos em várias posições no interior da câmara de vácuo e em diversos instantes durante o acionamento das bobinas de campos toroidal e poloidal. No final de 2001, com apenas 16% do total de capacitores instalado nos bancos, a corrente de plasma no ETE atingiu valores que variaram entre 35 e 45 kA com durações de pulso entre 4,5 e 3 ms, respectivamente.

Um conjunto básico de diagnósticos, compreendendo sinais de controle da máquina, espectroscópicos e magnéticos, encontra-se em condição operacional. O sistema de espalhamento Thomson foi montado e testado. A temperatura de plasma medida nas condições atuais de baixa energia dos bancos de capacitors situa-se na faixa compreendida entre 20 e 50 eV para diferentes condições da descarga. A sonda por feixe rápido de átomos de lítio foi montada, e testes da fonte e do canhão de íons de lítio estão em andamento.

Testes iniciais de um monotron de 6,7 GHz, 30 kW foram realizados. Medidas eletromagnéticas da cavidade fria confirmaram as previsões teóricas tanto para a freqüência e modo de operação da cavidade como para a eficiência de circuito. A primeira versão do canhão eletrônico apresentou problemas de aquecimento excessivo, o que levou à confecção de uma versão melhorada que deverá ser testada em breve.

Foram realizados trabalhos teóricos nas áreas de modelagem do circuito de potência e de transporte zero-dimensional do plasma, de simulação dos efeitos de corrente parasitas, e de cálculos auto-consistentes do equilíbrio de plasma.

Uma descrição completa das atividades realizadas dentro da linha de pesquisa e desenvolvimento em fusão foi feita durante o *Joint Meeting of the Second IAEA Technical Committee Meeting on Spherical Tori and the Seventh International Spherical Torus Workshop*, organizado pelo LAP e que teve lugar no Instituto Nacional de Pesquisas Espaciais no período entre 1 e 3 de agosto de 2001. Os trabalhos sobre o ETE apresentados durante este evento encontram-se no apêndice.

Metas para 2002

Muitas das atividades descritas acima deverão prosseguir durante o ano de 2002. Espera-se que a instalação dos bancos de capacitores seja finalizada visando atingir o patamar de 150 – 200

kA da corrente de plasma e 0,3 – 0,4 T do campo magnético toroidal. A operação do ETE será progressivamente otimizada possibilitando estudos do espaço de operação da máquina e de parâmetros do plasma. Testes da sonda por feixe de lítio e medidas iniciais dos parâmetros do plasma na borda do ETE serão realizados. O sistema de aquisição de dados será expandido e o número de sondas magnéticas aumentado de modo a possibilitar estudos iniciais de reconstrução magnética. Um conjunto adicional de limitadores de grafite será instalado na câmara de vácuo e procedimentos de limpeza da câmara terão prosseguimento. Será também iniciado o projeto e construção de partes dos sistemas de interferometria por laser no infravermelho longínquo e de imageamento de raios-X moles. O protótipo do monotron, dispositivo gerador de microondas para pré-ionização e aquecimento do plasma, será montado e testado. Os trabalhos nas áreas de equilíbrio, modelagem zero-dimensional da partida, simulação de fenômenos na borda e transporte neo-clássico do plasma deverão prosseguir durante o ano de 2002.

Comentários

O ETE é um dos poucos tokamaks esféricos em operação no mundo, sendo o LAP uma das instituições pioneiras no desenvolvimento deste conceito, a partir de 1986. Atualmente, só existem outras máquinas deste tipo em operação na Inglaterra, nos Estados Unidos, no Japão e na Rússia, e em planejamento na Itália e na China. O LAP mantém contato e colaboração com praticamente todos os grupos internacionais que atuam no desenvolvimento de toróides esféricos, configuração na qual estão concentrados os novos investimentos na área de pesquisa em confinamento magnético, tendo em vista os resultados satisfatórios já atingidos e sem levar em conta os investimentos ainda em discussão que serão empregados na construção do International Thermonuclear Experimental Reactor – Fusion Energy Advanced Tokamak (ITER-FEAT). Esta colaboração entre grupos de pesquisa é em grande parte promovida pela Agência Internacional de Energia Atômica – IAEA, com a qual o LAP mantém um contrato de pesquisa. Acordos específicos de colaboração também são mantidos pelo LAP com o Centro de Ciências de Culham, Inglaterra, com o Instituto Superior Técnico de Lisboa, Portugal, e com a Universidade de Fukui, Japão. Atualmente, as atividades do LAP na área de fusão estão direcionadas para colocação do ETE em condições de operação plena, pela expansão das fontes de potência e pela instalação de sistemas de diagnóstico de plasma e de aquisição de dados, de modo a transformá-lo num experimento de padrão internacional. Deve-se também lembrar que o grupo do LAP encarregado do desenvolvimento de fontes para pré-ionização e aquecimento do plasma é o único no país que mantém competência na área de microondas de alta potência, com reconhecimento internacional.

Dificuldades

As dificuldades na execução do projeto foram as mesmas encontradas de forma crônica em qualquer atividade de pesquisa, notadamente experimental, no Brasil: 1) indefinição na liberação dos recursos aprovados, geralmente acompanhada de cortes substanciais; 2) empecilhos burocráticos e administrativos que praticamente inviabilizam a pesquisa; 3) falta de continuidade, principalmente no que se refere à transferência de tecnologia para o setor produtivo e de conhecimentos para as futuras gerações; 4) descaso institucional pela área de Ciência e Tecnologia. Particularmente danoso foi o corte de 50% das bolsas MCT/PCI em meados de 2001, que desmantelou a equipe de apoio técnico do laboratório do tokamak ETE. No caso de um projeto como o ETE constata-se, além dos problemas citados, a inexistência de uma política voltada para a questão energética futura do País.

O ETE oferece a possibilidade do Brasil acompanhar o desenvolvimento internacional na área de dispositivos compactos de confinamento magnético para fusão. Entretanto, para assegurar este papel, e impedir que o experimento se torne rapidamente obsoleto, é necessário haver um aporte substancial e contínuo de recursos. É também essencial que haja contratação de novos pesquisadores para atuar, principalmente, nas áreas de desenvolvimento de diagnósticos e

interpretação de dados experimentais, controle e aquisição de dados, desenvolvimento e utilização de equipamentos para aquecimento de plasma, e desenvolvimento teórico e computacional. Além disso, a atualização e manutenção do experimento depende da contratação de engenheiros eletro-eletrônicos, bem como técnicos experientes em mecânica, eletrônica e de laboratório, em caráter mais permanente que o regime de bolsas.

Publicações – Participação em Congressos

- **Artigos Publicados em Periódicos**

BARROSO, J.J.; KOSTOV, K.G.; LEITE NETO, J.P. "An axial monotron with rippled wall resonator". *International Journal of Infrared and Millimeter Waves,* **22** (2), 265-276, February 2001.

BARROSO, J.J. "A triple-beam 6.7 GHz, 340 kW monotron". *IEEE Transaction on Electron Devices*, **48** (4) 815-817, April 2001.

BARROSO, J.J.; TERRA, M.O.; MACAU, E.E.N. "Bifurcation and chaos in the second instability window of the classical Pierce diode". *International Journal of Bifurcation and Chaos*, **11** (10) 251-260 (2001).

MONTEIRO, M.J.R.; MACHIDA, M.; DALTRINI, A.M.; BERNI, L.A. "Comparison of two multipass configurations for scattered light amplification". *Brazilian Journal of Physics*, **31**(3) 502-506, September 2001.

- **Artigos Aceitos para Publicação em Periódicos**

BARROSO, J.J.; KOSTOV, K.G. "Triple-beam monotron". Accepted for publication in *IEEE Transactions on Plasma Science.*

KOSTOV, K.G.; BARROSO, J.J. "Space-charge-limited current in cylindrical diodes with finite-length emitter". Accepted for publication in *Physics of Plasmas.*

OLIVEIRA, R.M.; UEDA, M.; VILELA, W.A. "Fast neutral lithium beam for density and its fluctuation measurements at the boundary regions of ETE tokamak". Accepted for publication in *Brazilian Journal of Physics*, 2001.

- **Artigos Submetidos para Publicação em Periódicos**

BARROSO, J.J.; LEITE NETO, J.P.; KOSTOV, K.G. "Cylindrical waveguide with axially rippled wall". Submitted to *IEEE Transactions Microwave Theory and Techniques.*

CASTRO, P.J.; BARROSO, J.J.; CORRÊA, R.A. "Measurement of electric field azimuthal distribution on gyrotron resonator". Submitted to *International Journal of Electronics*.

MONTEIRO, M.J.R.; MACHIDA, M.; DALTRINI, A.M.; BERNI, L.A. "Multichannel photomultiplier for multipass Thomson scattering diagnostics". Submitted to *Brazilian Journal of Physics, Proceedings of the 14th* IAE*A Technical Committee Meeting on Research Using Small Devices*, June 25-27, 2001, São Paulo, Brazil.

OLIVEIRA, R.M.; BARBOSA, L.F.W., FERREIRA, J.G.; SHIBATA, C.S. "Conceptual project and present status of the ETE control and data acquisiton systems". Submitted to *Fusion Engineering & Design.*

- **Publicações em Congressos Internacionais**

ANDRADE, M.C.R.; LUDWIG, G.O.; CAMARGO, S.J. "Current density components provided by a self-consistent equilibrium calculation in tokamak plasmas". Proceedings of the *10th International Congress on Plasma Physics – ICPP*, Quebec City, Canada, vol. II, pp. 620, January, 2001.

LUDWIG, G.O. "Approximate solutions of the Grad-Schlüter-Shafranov equation". *Fusion Energy 2000*, *18th Conference* Proceedings, paper THP2/16, p. 418 (5 pages), International Atomic Energy Agency, Vienna, May 2001.

BARBOSA, L.F.W.; FERREIRA, J.G.; LUDWIG, G.O.; DEL BOSCO**,** E.; ROSSI, J.O. "Pulsed electric system for production and confinement of plasma in ETE – Spherical Tokamak

Experiment". *Proceedings of the International Conference on Pulsed Power & Plasma Science*, June 17-22, 2001, Las Vegas, USA.

BARROSO, J.J.; KOSTOV, K.G. "The axial monotron as a high-power microwave tube". *Proceedings do International Conference on Pulsed Power & Plasma Science,* June 17-22, 2001, Las Vegas, USA.

BARROSO, J.J.; LEITE NETO, J.P.; KOSTOV. K.G. "An axial monotron with rippled wall resonator". *Proceedings do International Conference on Pulsed Power & Plasma Science,* June 17-22, 2001, Las Vegas, USA.

BARROSO, J.J.; CASTRO, P.J.; ROSSI, J.O.; PATIRE JR., H.; KOSTOV, K.G.; LUDWIG, G.O.; GONÇALVES, J.A.; SANDONATO, G.M.; LEITE NETO, J.P. "High-power microwave research at the Associated Plasma Laboratory of INPE for application in spherical tokamaks". *14th* IAE*A Technical Committee Meeting on Research Using Small Devices*, June 25-27, 2001, São Paulo, Brazil.

DEL BOSCO, E.; LUDWIG, G.O.; FERREIRA, J.G.; BERNI, L.A.; OLIVEIRA, R.M. SHIBATA, C.S.; PATIRE, H.; ROSSI, J.O.; VILELA, W.A.; BARBOSA, L.F.W. "ETE spherical tokamak – design and first results". *14th* IAE*A Technical Committee Meeting on Research Using Small Devices*, June 25-27, 2001, São Paulo, Brazil.

KOSTOV, K.G.; BARROSO, J.J. "Space-charge-limited current in cylindrical diodes with finite-length emitter". *14th* IAE*A Technical Committee Meeting on Research Using Small Devices*, June 25-27, 2001, São Paulo, Brazil.

LEITE NETO, J.P.; BARROSO, J.J.; KOSTOV, K.G. "Electrodynamical properties of axially corrugated waveguides". *14th IAEA Technical Committee Meeting on Research Using Small Devices*, June 25-27, 2001, São Paulo, Brazil.

OLIVEIRA, R.M.; UEDA, M.; VILELA, W.A. "Fast neutral lithium beam for density and its fluctuation measurements at the boundary regions of ETE tokamak". *14th IAEA Technical Committee Meeting on Research Using Small Devices*, June 25-27, 2001, São Paulo, SP, Brazil.

OLIVEIRA, R.M.; BARBOSA, L.F.W., FERREIRA, J.G.; SHIBATA, C.S. "Conceptual project and present status of the ETE control and data acquisiton systems". *3rd International Atomic Energy Agency Technical Committee Meeting on Control, Data Acquisition & Remote Participation for Fusion Research*, July 13-21, 2001, Padova, Italy.

CASTRO, P.J.; BARROSO, J.J.; LEITE NETO, J.P. "Resonance frequencies of cavities with sinusoidally rippled cross sections". *2001 International Microwave and Optoelectronics Conference*, August 6-10, 2001, Proceedings SBMO-IEEE, Belém, PA, 2001, p. 75-78.

ANDRADE, M.C.R.; LUDWIG, G.O. "Comparison of bootstrap current models in a self-consistent equilibrium calculation for tokamak plasmas". *Joint Meeting of the 2nd IAEA Technical Committee Meeting on Spherical Tori and the 7th International Spherical Torus Workshop,* 1-3 August, 2001, INPE, São José dos Campos, SP, Brazil.

BARROSO, J.J.; CASTRO, P.J.; ROSSI, J.O.; PATIRE JR., H.; KOSTOV, K.G.; LUDWIG, G.O.; GONÇALVES, J.A.; SANDONATO, G.M.; LEITE NETO, J.P. "Development of a high-power monotron for RF applications in spherical tokamaks". *Joint Meeting of the 2nd IAEA Technical Committee Meeting on Spherical Tori and the 7th International Spherical Torus Workshop,* 1-3 August, 2001, INPE, São José dos Campos, SP, Brazil.

BERNI, L.A.; MACHIDA, M.; DEL BOSCO, E.; MONTEIRO, M.J.R.; OLIVEIRA, R.M.; VILELA, W.A.; UEDA, M.; CIOBAN, D.; DALTRINI, A.M.; CASTRO, R.M.; FERREIRA, J.G.; LUDWIG, G.O. "Present status of ETE diagnostics". *Joint Meeting of the 2nd IAEA Technical Committee Meeting on Spherical Tori and the 7th International Spherical Torus Workshop*, 1-3 August, 2001, INPE, São José dos Campos, SP, Brazil.

DEL BOSCO, E.; FERREIRA, J.G.; BERNI, L.A.; OLIVEIRA, R.M.; LUDWIG, G.O.; SHIBATA, C.S.; PATIRE JR., H.; ROSSI, J.O.; VILELA, W.A.; BARBOSA, L.F.P. W. "Overview of the ETE spherical tokamak". *Joint Meeting of the 2nd IAEA Technical Committee Meeting on Spherical Tori*

and the 7th International Spherical Torus Workshop, 1-3 August, 2001, INPE, São José dos Campos, SP, Brazil.

GRISHANOV, N.I.; AZEVEDO, C.A.; LUDWIG, G.O.; NETO, P.J. "Radio frequency wave dissipation by electron Landau damping in elongated spherical tokamaks". *Joint Meeting of the 2nd IAEA Technical Committee Meeting on Spherical Tori and the 7th International Spherical Torus Workshop,* 1-3 August, 2001, INPE, São José dos Campos, SP, Brazil.

NAKAMURA, K.; IGUCHI, H.; UEDA, M. et al. "Two dimensional measurement using lithium beam probe at the helical divertor region in CHS(I)". *Annual Meeting of Plasma and Nuclear Fusion*, November 27-30, 2001, Fukuoka, Japan.

- **Resumos em Congressos Internacionais**

BARBOSA, L.F.P.W.; OLIVEIRA, R.M.; SHIBATA, C.S.; FERREIRA, J.G. "ETE control and data acquisiton system". *14th IAEA Technical Committee Meeting on Research Using Small Fusion Devices*, USP, p. 45, São Paulo, June 25-27, 2001.

- **Resumos em Congressos Nacionais**

BERNI, L.A.; DEL BOSCO, E.; LOBO, M.F.G. "First results of wall conditioning on the ETE spherical tokamak". *XXII Congresso Brasileiro de Aplicações de Vácuo na Indústria e na Ciência – XXII CBRAVIC*, p. 44, 25-27 de julho de 2001, UNESP, Campus de Guaratinguetá, Guaratinguetá, SP.

MONTEIRO, M.J.R.; MACHIDA, M.; DALTRINI, A.M.; CIOLAN, D.; BERNI, L.A. "Use of a 10 stage 64 channel photomultiplier tube for low-light scattering diagnostics". *XXII Congresso Brasileiro de Aplicações de Vácuo na Indústria e na Ciência – XXII CBRAVIC*, p. 56**,** 25-27 de julho de 2001, UNESP, Campus de Guaratinguetá, Guaratinguetá, SP.

OLIVEIRA, R.M.; UEDA, M. "Investigation of Li^+ thermionic sources for fast neutral lithium beam probing". *XXII Congresso Brasileiro de Aplicações de Vácuo na Indústria e na Ciência – XXII CBRAVIC*, p. 57, 25-27 de julho de 1002, UNESP, Campus de Guaratinguetá, Guaratinguetá, SP.

DEL BOSCO, E.; FERREIRA, J.G.; BERNI, L.A. "Plasma formation in the ETE spherical tokamak". *XXII Congresso Brasileiro de Aplicações de Vácuo na Indústria e na Ciência – XXII CBRAVIC*, p. 59, 25-27 de julho de 2001, UNESP, Campus de Guaratinguetá, Guaratinguetá, SP.

BARROSO, J.J.; CASTRO, P.J.; ROSSI, J.O.; PATIRE JR., H.; KOSTOV, K.G.; LUDWIG, G.O.; GONÇALVES, J.A.; SANDONATO, G.M.; LEITE NETO, J.P. "Monotron development for application in spherical tokamaks". *XXII Congresso Brasileiro de Aplicações de Vácuo na Indústria e na Ciência – XXII CBRAVIC***,** p. 60, 25-27 de julho de 2001, UNESP, Campus de Guaratinguetá, Guaratinguetá, SP.

LEITE NETO, J.P.; BARROSO, J.J.; CASTRO, J.P. "Eigenmodes and ohmic losses in cylindrical cavity resonators with sinusoidally rippled cross sections". *6º Encontro Brasileiro de Física dos Plasmas*, p. 26, 1-5 dezembro, 2001, Campos do Jordão, SP.

PATIRE, H. JR., BARROSO, J.J.; CASTRO, P.J.; ROSSI, J.O.; LUDWIG, G.O.; GONÇALVES, J.A.; SANDONATO, G.M. "Design and construction of a 20A, 10kV injection electron gun". *6º Encontro Brasileiro de Física dos Plasmas*, p. 26, 1-5 dezembro, 2001, Campos do Jordão, SP.

CASTRO, P.J.; BARROSO, J.J.; LEITE NETO, J.P. "Azimuthally corrugated cavities for harmonic gyrotron". *6º Encontro Brasileiro de Física dos Plasmas*, p. 32, 1-5 dezembro, 2001, Campos do Jordão, SP.

LUDWIG, G.O.; DEL BOSCO, E.; FERREIRA, J.G.; BARROSO, J.J.; BERNI, L.A.; OLIVEIRA, R.M. "First results of the ETE Spherical Torus". *6º Encontro Brasileiro de Física dos Plasmas*, p. 53, 1-5 dezembro, 2001, Campos do Jordão, SP.

ANDRADE, M.C.R.; LUDWIG, G.O. "Different bootstrap current and plasma conductivity models applied in a self-consistent equilibrium calculation for tokamak plasmas". *6º Encontro Brasileiro de Física dos Plasmas*, p. 55, 1-5 dezembro, 2001, Campos do Jordão, SP.

BERNI, L.A.; UEDA, M.; DEL BOSCO, E. “Present status of the Thomson scattering diagnostic for Tokamak ETE”. *6º Encontro Brasileiro de Física dos Plasmas*, p. 59, 1-5 dezembro, 2001, Campos do Jordão, SP.

BARBOSA, L.F.W.; LUDWIG, G.O. “Aplicação e testes de redes neurais artificiais em sistema de levitação magnética para futura aplicação no controle vertical de plasma em tokamaks". *6º Encontro Brasileiro de Física dos Plasmas*, p. 59, 1-5 dezembro, 2001, Campos do Jordão, SP.

OLIVEIRA, R.M.; UEDA, M.; BERNI, L.A. “Development of a fast neutral lithium beam diagnostic to probe the edge plasma of the ETE tokamak”. *6º Encontro Brasileiro de Física dos Plasmas*, p. 61, 1-5 dezembro, 2001, Campos do Jordão, SP.

- **Relatórios Técnicos Internos**

BARBOSA, L.F.P.W.; LUDWIG, G.O. “Redes neurais no modelamento e controle de tokamaks – aplicação ao ETE (Experimento Tokamak Esférico) – Terceiro Relatório”. INPE-8477-PRP/226, novembro 2001.

- **Outros Trabalhos**

CASTRO, P.J. “Monotron e cavidades azimutalmente corrugadas: aplicação à geração de microondas de alta potência”. Projeto individual de Pesquisa submetido e aprovado pela Fundação de Amparo à Pesquisa do Estado de Paulo – FAPESP, processo nº 2001/02496-6, março 2001.

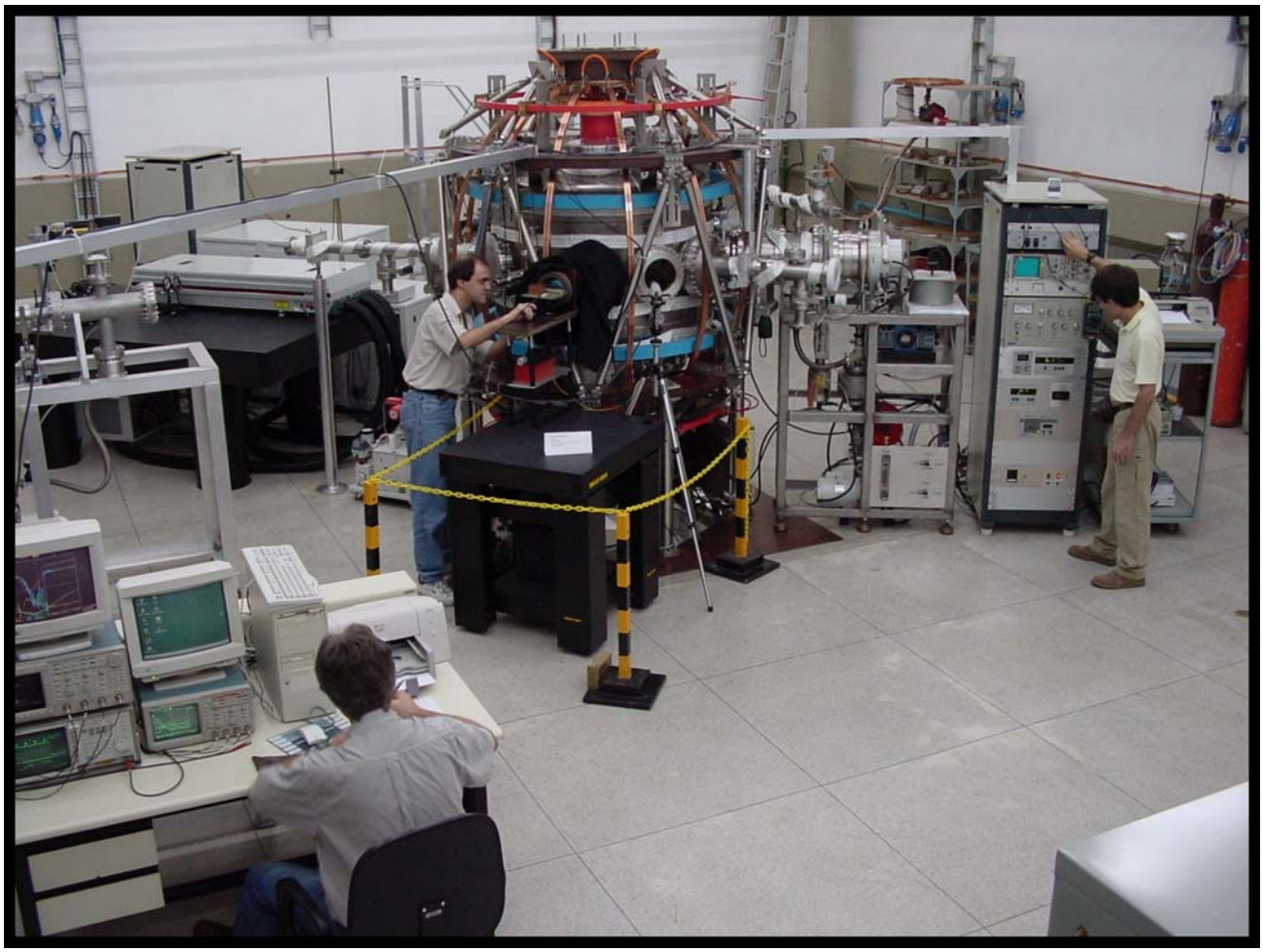

Vista geral do tokamak esférico ETE em Novembro de 2001.

Apêndice

Trabalhos realizados dentro da linha de pesquisa e desenvolvimento em fusão termonuclear controlada que foram apresentados durante o *Joint Meeting of the Second IAEA Technical Committee Meeting on Spherical Tori and the Seventh International Spherical Torus Workshop*, São José dos Campos, SP, 1 a 3 de agosto de 2001:

- ANDRADE, M.C.R.; LUDWIG, G.O. "Comparison of bootstrap current models in a self-consistent equilibrium calculation for tokamak plasmas".
- BARROSO, J.J.; CASTRO, P.J.; ROSSI, J.O.; PATIRE JR., H.; KOSTOV, K.G.; LUDWIG, G.O.; GONÇALVES, J.A.; SANDONATO, G.M.; LEITE NETO, J.P. "Development of a high-power monotron for RF applications in spherical tokamaks".
- BERNI, L.A.; MACHIDA, M.; DEL BOSCO, E.; MONTEIRO, M.J.R.; OLIVEIRA, R.M.; VILELA, W.A.; UEDA, M.; CIOBAN, D.; DALTRINI, A.M.; CASTRO, R.M.; FERREIRA, J.G.; LUDWIG, G.O. "Present status of ETE diagnostics".
- DEL BOSCO, E.; FERREIRA, J.G.; BERNI, L.A.; OLIVEIRA, R.M.; LUDWIG, G.O.; SHIBATA, C.S.; PATIRE JR., H.; ROSSI, J.O.; VILELA, W.A.; BARBOSA, L.F.P. W. "Overview of the ETE spherical tokamak".
- GRISHANOV, N.I.; AZEVEDO, C.A.; LUDWIG, G.O.; NETO, P.J. "Radio frequency wave dissipation by electron Landau damping in elongated spherical tokamaks".

Comparison of Bootstrap Current Models in a Self-Consistent Equilibrium Calculation for Tokamak Plasmas

M. C. R. Andrade* and G. O. Ludwig

Instituto Nacional de Pesquisas Espaciais, POBox 515, 12201-970, São José dos Campos, SP, Brazil
**E-mail: mcr@plasma.inpe.br*

1. Introduction. Different bootstrap current formulations are employed in a self-consistent equilibrium for tokamak plasmas where the total plasma current profile is supposed to have contributions of the diamagnetic, Pfirsch-Schlüter, and the neoclassical ohmic and bootstrap currents [1]. A comparison among the different bootstrap current models is performed for a variety of plasma parameters of the small aspect ratio tokamak ETE (*Experimento Tokamak Esférico*) [2], placed at the Associated Plasma Laboratory of INPE, in Brazil. The calculations described here were performed using the Mathematica package in a PC type computer.

2. Equilibrium and Self-Consistent Calculation. A self-consistent equilibrium calculation, valid for arbitrary aspect ratio tokamaks, is obtained through a direct variational technique where the extremum of the functional given by the internal plasma energy represents the flux surface averaged Grad-Shafranov equation (GS) being, in this way, a solution to the plasma equilibrium. This extremum establishes a relation between the total poloidal current, $I(\rho)$, between the symmetry axis and a given magnetic surface, denoted by the radial coordinate ρ, and the total plasma current enclosed by this surface, $I_T(\rho)$, as follows [1]:

$$I_T(\rho)\,\frac{dI_T}{d\rho} = -K(\rho)\,\frac{dL}{d\rho}\,I(\rho)\,\frac{dI}{d\rho} - K(\rho)\,\frac{dV}{d\rho}\frac{dp}{d\rho}\ , \qquad (1)$$

where $p(\rho)$ is the total plasma pressure profile and $L(\rho)$, $V(\rho)$ and $K(\rho)$ are, respectively, the inductance of the toroidal solenoid coincident with a given flux surface, the volume involved by this surface and the inverse kernel used to calculate the self-inductance of the plasma loop. The self- consistent calculation requires that the current profile which satisfies Eq. (1), has also to be given by the sum of all current components, described by:

$$-I\,\frac{dI}{d\rho} = \frac{I_T(\rho)}{K(\rho)}\left[\frac{\left\langle \vec{J}_{oh}\cdot\vec{B}\right\rangle}{\left\langle B^2\right\rangle}\,I + \frac{\left\langle \vec{J}_{bs}\cdot\vec{B}\right\rangle}{\left\langle B^2\right\rangle}\,I\right] + \frac{\mu_0 I^2}{\left\langle B^2\right\rangle}\,\frac{dp}{d\rho}\ , \qquad (2)$$

where the first term on the *rhs* of Eq.(2) refers to the ohmic current (oh) modified by neoclassical effects through the plasma conductivity, the second term to the bootstrap current (bs) calculated through different models as described in the next section and the last term results from a combination of the diamagnetic (dia) and the Pfirsch-Schlüter (ps) currents. The brackets in Eq.(2) refer to the usual flux surface average and $\vec{B}$ is the total induction in the plasma. The self-consistent equilibrium is obtained when Eq.(2) is solved iteratively with Eq.(1) as described in [1]. The loop voltage that enters in the ohmic current calculation is determined consistently in order to reproduce the prescribed value of the total plasma current.

3. Bootstrap Current Models. Different bootstrap current models are listed in Table 1 and classified according their validity regarding aspect ratio, collisionality or plasma impurity level. The full matrix Hirshman-Sigmar (H-S) formulation for the bootstrap current estimate is based on the solution of the system formed by the flux surface average of the parallel momentum and heat flow balance equations for each species in the plasma, as follows [3]:

$$\mu_{a1}\left\langle u_{a//}\,B\right\rangle-\mu_{a1}\,V_{a1}\,B+\frac{2}{5}\mu_{a2}\left\langle\frac{q_{a//}}{p_a}B\right\rangle-\mu_{a2}\,V_{a2}\,B\;=\;\sum_b\left(l_{11}^{ab}\left\langle u_{b//}B\right\rangle-\frac{2}{5}l_{12}^{ab}\left\langle\frac{q_{b//}}{p_b}B\right\rangle\right)\qquad(3)$$

$$\mu_{a2}\left\langle u_{a//}\,B\right\rangle-\mu_{a2}\,V_{a1}\,B+\frac{2}{5}\mu_{a3}\left\langle\frac{q_{a//}}{p_a}B\right\rangle-\mu_{a3}\,V_{a2}\,B\;=\;\sum_b\left(-l_{21}^{ab}\left\langle u_{b//}B\right\rangle+\frac{2}{5}l_{22}^{ab}\left\langle\frac{q_{b//}}{p_b}B\right\rangle\right)\qquad(4)$$

The solution of this system provides the parallel fluid $<u_{a//}B>$ and heat $<2q_{a//}/5p_a>$ flows for each species in terms of the thermodynamic flows (described through V_{a1} and V_{a2}) and determines the bootstrap current through the expression $\langle J_{bs}\cdot B\rangle=\sum_a n_a e_a\langle u_{a//}B\rangle$, where n_a and e_a are respectively the density and charge of species a. The Hirshman-Sigmar model is therefore suitable for a multi-species plasma treatment since the equations in the system above are added accordingly as the number of plasma species increases. l_{ij}^{ab} are the friction coefficients, which are independent of the magnetic field configuration and so, valid in all collision frequency regimes. Their formulae are found in [3]. The problem is then to calculate the viscosity coefficients μ_{aj}, since they depend on the plasma geometry and collisionality. We will make a comparison among the H-S [3], Shaing [4] and Sauter´s [5] proposals regarding this calculation.

In order to compute the viscosity coefficients, the Hirshman-Sigmar model solves the linearized drift kinetic (ldk) equation asymptotically in each collisionality regime and proposes a formula continuously valid throughout the various regimes. However, in the plateau regime the result is valid only for large aspect ratios. Shaing solves the ldk equation where the mass velocity appears explicitly. The asymptotic values of his coefficients converge to the same values given by the Hirshman-Sigmar model in the Pfirsch-Schlüter and in the banana regimes, when the H-S banana coefficient is corrected by a $1/f_c$ factor in order to reproduce the correct limit in the finite aspect ratio banana regime (f_c is the fraction of circulating particles in the plasma). In the plateau regime Shaing´s coefficients are different from those derived by Hirshman-Sigmar. Both the H-S and Shaing´s models consider, however, an approximated Coulomb collision operator which can introduce errors up to 20% in the viscosity coefficients in the Pfirsch-Schlüter regime [3], which could be a problem mainly in trying to model the plasma edge. Finally, Sauter solves ldk´s equations for electrons and a single-ion species without considering plasma flows. In order to solve these ldk´s equations, Sauter uses an adjoint formalism and does not make any assumption regarding different collisionality regimes being, in this respect, completely general. Moreover, Sauter considers the full Coulomb collision operator and solves the adjoint equations varying aspect ratio, collisionality and ion charge Z. In this way, he proposes fitted formulae for the bootstrap current and for the neoclassical conductivity, whose expressions depend basically on these three parameters. For more accurate formulas regarding the ion charge dependence, Sauter should solve the adjoint equations for electrons and for each ion species as it is stressed in his paper. Multi-species effects are therefore approximately treated in his formulation by substituting the ion charge Z by the effective ion charge in the plasma (Z_{eff}). All the equations describing these models are found respectively in [3,4,5].

Models	Aspect Ratio	Collisionality	Impurities
Hinton-Hazeltine	large	all	Single-ion (Z_{eff})
Hirshman	all	banana regime	Single-ion (Z_{eff})
Hirshman-Sigmar	large	all	Multi-Species
Shaing	all	all	Multi-Species
Sauter	all	all	Single-ion (Z_{eff})

Table 1: Different formulations for the bootstrap current estimate

4. Results and Discussions. Bootstrap current estimates provided by the full matrix Hirshman-Sigmar model with the viscosity coefficients given by Shaing (H-S/Shaing model) and by the fitted formulae proposed by Sauter, both for the bootstrap current and for the neoclassical

conductivity, are presented for the ETE low aspect ratio tokamak [2]. For Shaing´s model, we compute the neoclassical conductivity according to the Hirshman, Hawryluk and Birge (HHB) formulation [6]. In both cases, the trapped particle fraction is estimated according to Lin-Liu and Miller [7]. The main ETE parameters correspond to aspect ratio $A=R_0(a)/a=1.5$, major radius $R_0(a)=0.3$ m, plasma current $I_p=200$ kA, vacuum toroidal field $B_T=0.4$ T (at $R_0(a)=0.3$ m), and plasma beta during the ohmic phase β=4-10%. The pressure, electron and ion temperature profiles were taken as gaussian shaped functions as in $f(\rho) = f(0) \exp[-\alpha_f (\rho/(w_f-\rho))^2]$, where f(0) determines the profile value at the axis, whereas α_f and w_f determine the value at the boundary. We have also considered $T_e(0) = T_i(0)$, $T_e(a) = T_i(a) = 0.03$ keV and $\alpha_{Te} = \alpha_{Ti} = 0.2$. As the pressure profile is given as a fixed input in our code, the density profiles were derived from the fact that the total pressure in the plasma is $p = n_e T_e + \sum_k n_k T_k$ and from the quasi-neutrality condition ($n_e = \sum_k n_k Z_k$), with the summations taken over all ion species. In Table 2, results provided by the self-consistent calculation for hydrogen plasmas in the ETE tokamak, lead to bootstrap current fractions roughly ranging from 10 to 35% for both models analysed according to the optimization level of the plasma parameters. We can also observe, by comparing cases II and V, that plasmas with higher shaped factors (higher elongation $\kappa(a)$ in our case) generate higher fractions of bootstrap current and that the presence of 2% of carbon in the plasma (Z_{eff}=1.54) causes a slight decrease in the bootstrap current fraction as noticed from cases II and III. Sauter predicts slightly higher fractions of bootstrap current in relation to the H-S/Shaing model in all cases analysed. The highest difference between the two models occurs for case IV (more collisional with ($T_e(0) = 200$ eV)). This may be due a combined effect resulting from the fact that Sauter uses the complete Coulomb collision operator whereas Shaing uses the approximated one, and that Shaing´s viscosity coefficients are derived from a different drift-kinetic equation which may result in differences in relation to Sauter´s, mainly in the transition banana-plateau or plateau-Pfirsch-Schlüter regimes.

	p(0) (kPa)	**$T_{e,i}(0)$ (keV)**	**α_p**	**$\kappa(a)$**	**$I_T(a)$(kA)**	**Z_{eff}**	**β_I**	**β_0**	**$I_{bsShaing}/I_T(a)$**	**$I_{bsFIT}/I_T(a)$**
I	15	0.5	3.0	2.0	200	1.54	0.54	0.09	**0.36**	**0.37**
II	10	0.4	3.0	2.0	200	1.00	0.36	0.06	**0.23**	**0.25**
III	10	0.4	3.0	2.0	200	**1.54**	0.36	0.06	**0.22**	**0.24**
IV	10	**0.2**	3.0	2.0	200	1.00	0.36	0.06	**0.14**	**0.20**
V	10	0.4	3.0	**1.7**	200	1.00	0.31	0.06	**0.17**	**0.19**
VI	10	0.4	3.0	**1.7**	**180**	1.54	0.38	0.06	**0.22**	**0.23**

Table 2: Plasma parameters for bootstrap current estimate provided by the self-consistent calculation

Figure 1 shows the total equilibrium current density profiles and all their different components for case II in Table 2, both for the bootstrap current obtained from the H-S/Shaing model (1a) and from the fitted formula proposed by Sauter (1b). For the H-S/Shaing model the neoclassical conductivity used in the ohmic current calculation is obtained from the HHB formulation [6] whereas in (1b) we have used Sauter´s fitted fomula [5]. Figure 2 shows the comparison of the bootstrap current profiles obtained from different models for cases II, III and IV. We can observe that, as the plasma becomes less collisional (higher temperatures in the cases shown) all the models approach each other. For figures 2a and 2b, the Hirshman collisionless model [8] always predicts more bootstrap current since it does not take properly into account the collisionality dependence on the viscosity coefficients. Still comparing figures 2a and 2b we see that as the Z_{eff} increases the H-S/Shaing and Sauter´s models approach each other. The strongest difference between the two predictions (fig. 2c) occurs for the most collisional case ($T_e(0) = 200$ eV) as previously mentioned. For the less collisional plasma (fig.2d) all the models agree quite well. The self-consistent calculation

generated when the bootstrap current is determined by the fitted formulae is approximately four times faster to compute than that provided when the H-S/Shaing model is used. Finally, figure 3 shows the neoclassical and Spitzer conductivities calculated for the HHB formulation and from the fitted formula, for case II, after the self-consistent calculation is achieved and obtained for the bootstrap current calculated according to Sauter. The figure also shows the reduction of the neoclassical conductivity in relation to Spitzer´s.

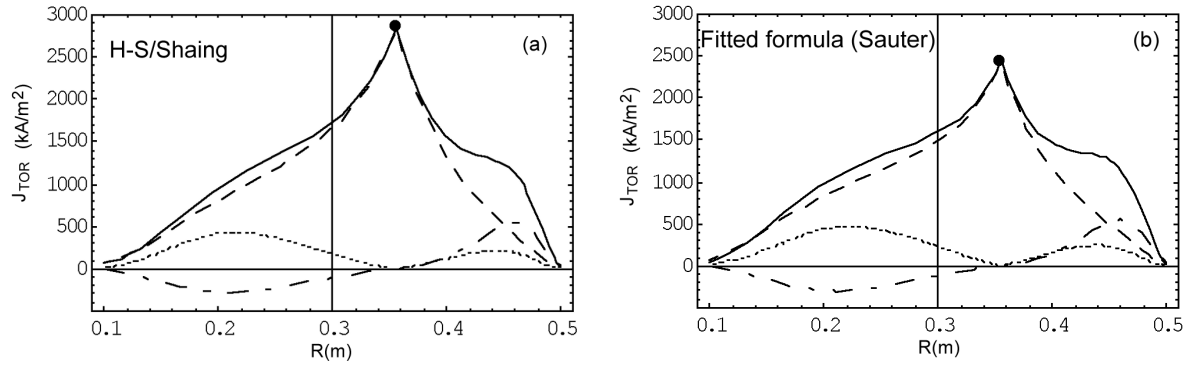

Figure 1: Current density profiles for case II in Table 2.The full line corresponds to the total equilibrium current density, the dashed line is the ohmic contribution, the dash-dotted line is the sum of the diamagnetic and Pfirsch-Schlüter components and the dotted line represents the boostrap current contribution.

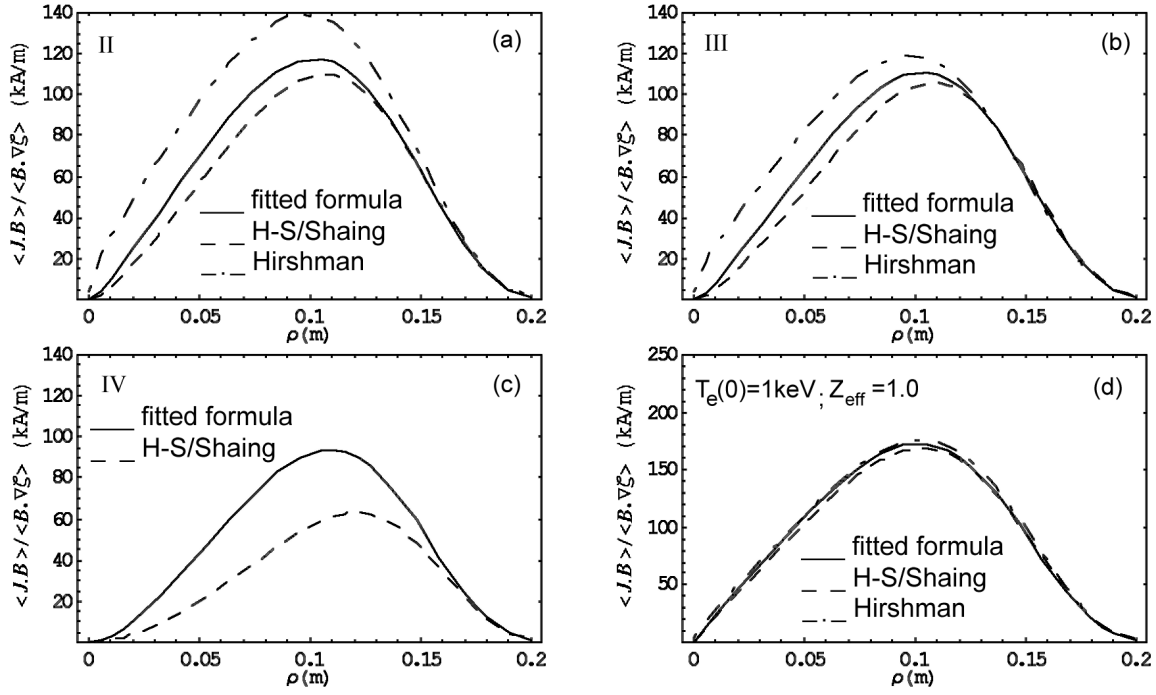

Figure 2: Bootstrap current profiles obtained from different models

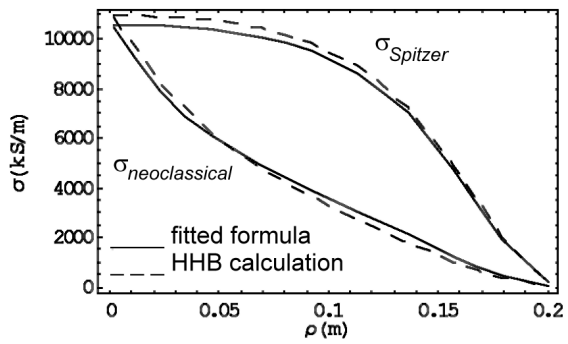

Figure 3: Neoclassical and Spitzer conductivities

References

[1] Andrade M.C.R., Ludwig G. O. and Camargo S.J., *Plasma. Phys. and Control. Fusion* **42**, 1269 (2000).

[2] Del Bosco E. et al, *Overview of the ETE Spherical Tokamak* in this workshop.

[3] Hirshman S.P, Sigmar, D. J., *Nuclear Fusion* **21**, 1079 (1981).

[4] Shaing K. C. et al, *Phys.Plasmas* **3**, 965 (1996).

[5] Sauter O. et al, *Phys. Plasmas* **6**, 2834 (1999).

[6] Hirshman S. P. et al, *Nuclear Fusion* **17**, 611 (1977).

[7] Lin-Liu Y. R. and Miller R. L., *Phys. Plasmas* **2**, 1666 (1995).

[8] Hirshman, S.P., *Phys. Fluids* **31**, 3150 (1988).

Development of a High-Power Monotron for RF Applications in Spherical Tokamaks

J. J. Barroso, K. G. Kostov, P. J. Castro, J. O. Rossi, H. Patire, Jr., G. O. Ludwig, J. A. Gonçalves, G. M. Sandonato, and J. P. Leite Neto

Associated Plasma Laboratory, INPE, P.O. Box 515, São José dos Campos, SP, Brazil

Abstract: Electron cyclotron heating (ECH) assist has been demonstrated to significantly improve startup performance of tokamaks by decreasing the loop voltage, which translates into ramp current rates higher than those of pure Ohmic startup at equivalent loop voltages. This has been observed on several machines that normally rely on the use of gyrotrons or an assembly of klystrons to produce such beneficial effects at particular electron cyclotron resonance frequencies. However, specific RF source requirements in terms of frequency and power demand specially customized designs, leading to costly industrial tubes. In light of these considerations, pre-ionization and plasma production on the ETE spherical tokamak of LAP/INPE are currently being pursued on the basis of the monotron, which, consisting of an electron beam that traverses a standing-wave cavity resonator, ranks as the simplest microwave tube. Thus describing the design, construction techniques and simulation results of a high-power microwave tube, the present paper reports on a proof-of-principle monotron experiment currently under way at our laboratory.

1. Introduction

Having been known since the 1930s [1,2], the monotron is a transit-time oscillator where the beam electrons cross the interaction space in a transit angle close to $(4k+1)\pi/2$ where k is an integer. Under this synchronism condition, the beam can interact unstably with a cavity mode, causing the RF field to grow at the expense of the DC beam energy [3,4]. Electron bunches are formed in the beam and reach the cavity end plate in a decelerating phase of the RF field thus transferring energy to the cavity RF field. The bunches constitute a fluctuating component of the convection current that induces in the resonator walls an RF current to sustain the oscillations. The present paper addresses the monotron by examining its capabilities regarding high efficiency operation with three hollow concentric beams to produce hundreds of kilowatt power output.

2. High-Efficiency Operating Regime

The analysis developed in this section is a one-dimensional Lagrangian treatment in which a representative number of electrons injected at the input plane is traced through the cavity taking account of the presence of a standing-wave electric field. Neglecting the space-charge forces between the charged particles in the beam, the normalized force equation is written as

$$\frac{d\tilde{p}}{d\tilde{t}} = \left[\frac{A}{\tilde{d}}\frac{\varepsilon_0}{mc^2}\right]\cos(\tilde{t}+\varphi)\cos(l\pi\tilde{z}/\tilde{d}) \tag{1}$$

with

$$\frac{d\tilde{z}}{d\tilde{t}} = \frac{\tilde{p}(t)c}{\sqrt{m^2c^2+\tilde{p}^2}} \tag{2}$$

where $\tilde{p} = p(t)/mc$ is the normalized electron momentum, with the time normalized as $\tilde{t} = 2\pi t/T$ and the distance as $\tilde{z} = z\omega/c$, q= -e and m are the electronic charge and the electron rest mass, φ specifies the electron entrance phase, l is an integer number defining the field distribution along the normalized interaction length $\tilde{d} = d\omega/c$; $\varepsilon_0 = qV_0$ denotes the initial energy of the injected beam, where V_0 is beam voltage; $A=V/V_0$ is defined as the field amplitude parameter where $V=E/d$ is the maximum RF voltage established across the cavity.

Given an axial number l and specifying the initial electron momentum, we infer that the final momentum of a single electron upon reaching the collector plate at $z=d$ on a transit time $\tau(\varphi)$ is determined by the entrance phase φ and by the set of parameters $\tilde{d}$, A, and ε_0 . The corresponding final kinetic energy for a single electron is

$$\varepsilon_s(\tau) = mc^2\left(\sqrt{1+(p(\tau)/mc)^2}-1\right) \tag{3}$$

and the kinetic energy of the exit beam at $z=d$ is calculated by averaging out the individual electron energies over the phase φ

$$\langle \varepsilon_B \rangle = \frac{1}{2\pi}\int_0^{2\pi}\varepsilon_s(\tau)d\varphi = \frac{1}{N}\sum_{k=1}^{N}\varepsilon_{k,s}(d) \tag{4}$$

where N is the total number of electrons injected during a period T. The electronic efficiency is expressed by $\eta_{el} = 1-\langle \varepsilon_B \rangle/\varepsilon_0$. On account of (1) the efficiency is seen to be a function of the normalized quantities A, $\tilde{d}$, and ε_0 , i.e. $\eta_{el} = \eta_{el}(A,\tilde{d},\varepsilon_0)$ for a given index l specifying the electric field axial profile. If η_{el} thus calculated is positive, then the electrons transfer energy to the RF field. In what follows, the electronic efficiency is maximized and given as a function of the single parameter $\tilde{d}$. The input beam energy ε_0 and the axial number l are fixed and (1) is numerically integrated using the optimum value of the amplitude parameter A such that a maximum efficiency is calculated from (4) with N=500.

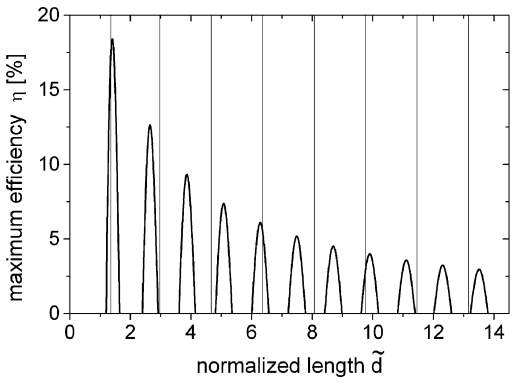

Fig. 1. *Maximum electronic efficiency vs normalized length $\tilde{d}$ for l=0, ε_0=10keV, and A=3.9.*

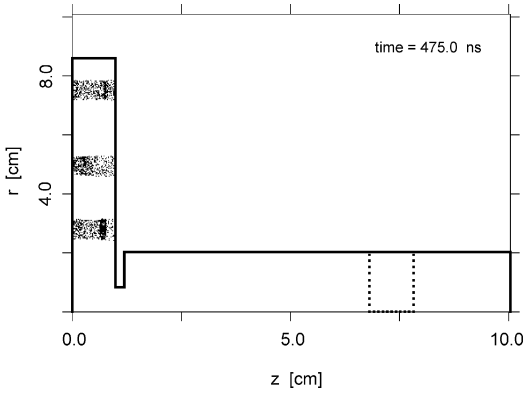

Fig. 2 *Simulation configuration of the triple-beam monotron, showing bunched beams.*

Considering ε_0 = 10keV and l=0 modes, a typical tuning curve is shown in Fig.1. This figure brings a discrete set of beam modes with $\eta_{el,\max}$ peaking at evenly spaced values of $\tilde{d}$ i.e., $\tilde{d}_{\max}$ =1.4, 2.6, 3.8,…. For comparison purposes, the vertical lines dropping to the $\tilde{d}$ -axis in Fig. 1 indicate the resonant frequencies of the TM_{0n0}, n=1,2,3,...,11 modes in a circular cylindrical cavity of length d=1.0 cm and radius R_w=1.85 cm.

The maximum efficiency, at ε_0 =10keV, reaches 18.5% for operation in l=0 modes at $\tilde{d}$ =1.4 as illustrated by Fig. 1. In this condition, the optimum DC electron transit time τ_0 has been found to be $\tau_0 \approx$ (n+0.15)T with n=1,2,...,11 corresponding to the beam modes in Fig. 1. It is seen that the cavity parameter $\tilde{d}$ =1.3 corresponding to the resonating TM_{010} mode (n=1) in the test cavity is somewhat less than the optimum $\tilde{d}$ =1.4 required by the 10-keV electron beam, since the vertical frequency line passes on the left of the highest efficiency peak at $\tilde{d}$ =1.4. Instead of lowering ε_0 , which is equivalent to shifting the whole beam spectrum to the left, an alternate approach to provide the optimum cavity-beam coupling is to increase the

cavity $\tilde{d}$ from 1.3 to 1.4. Noting that $\tilde{d} = d\omega / c$ and that the cavity radius R_w is determined from the boundary condition, $R_W(cm) = (15/\pi)\chi_{0n} / f(GHz)$ one gets $R_W = \chi_{0n} d / \tilde{d}$ where χ_{0n} denotes the *n-th* zero of the Bessel function J_0. Keeping constant the interaction length d=1.0 cm, and considering operation in the TM_{010} mode (χ_{01}=2.4048), the cavity radius has to be decreased from 1.85 cm to 1.72 cm for optimum operation. Selecting, however, the higher order TM_{040} mode χ_{04}=11.7915 the required cavity radius is calculated as R_w=8.42cm.

3. Triple-Beam Monotron

This Section describes the nominal geometry of a monotron having three annular beams at the maxima of the radial distribution of the electric field in a TM_{040}-mode cavity with a circular aperture through which electromagnetic energy stored in the resonant cavity is extracted to the output guide. At an injection beam energy $\varepsilon_0 = 10keV$, the optimum cavity dimensions of the monotron considered here have been determined in the previous section as length d=1.0cm and radius R_w=8.42cm, which gives a resonant frequency $f = (15/\pi)(p_{04} / R_w(cm))$=6.68GHz, and normalized length $\tilde{d} = 1.4$. By viewing the cavity as a short-circuited diode, the beams are injected from the left and run in the temperature-limited regime with each current in proportion to the area of the beams' cross-section, i.e., $I_I = J_c/\pi[r_{2,i}^2 - r_{1,i}^2]$ where J_c is the current density. The beams are 0.4-cm thick and centered at the positions r=2.8, 5.1, and 7.4 cm, which correspond to three consecutive maxima of the radial electric field distribution for the TM_{04} mode in an empty circular cavity. As depicted in Fig. 2, the resonant cavity is aperture coupled by means of a circular iris that transmits the RF power generated in the cavity to the 2.0-cm-radius output guide in which the lowest order TM_{01} mode propagates down. In the waveguide, a resistive disk is inserted having a resistance per unit square equal to the characteristic wave impedance of the TM_{01} output wave to absorb completely the incident wave[4].

4. PIC Code Simulation Results

By considering two values of R_I namely 0.8 cm and 0.9 cm in the monotron configuration of Fig. 2, the results given in this section encompass the overall efficiency η and average output power P_{out} over a total current range. The output power and total efficiency have been calculated from particle-in-cell (PIC) simulations. The program used is the KARAT code [5], that is based on 2½-D axisymmetric PIC model in which the Maxwell's equations and the equation of motion for macroparticles are solved self-consistently. The physical system is run on a grid with square cells 1 mm size with over three thousand macroparticles representing each beam in the configuration space as shown in Fig. 2 during steady state when the electron beams become fully density-modulated.

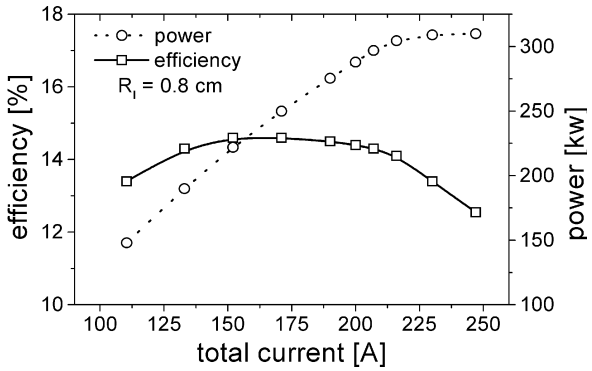

Fig. 3. *Dependence of output power and overall efficiency on total current for R_I=0.8 cm.*

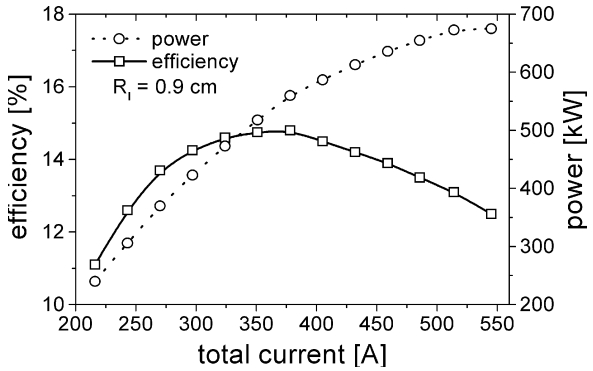

Fig. 4. *Dependence of output power and overall efficiency on total current for R_I= 0.9 cm.*

For R_I=0.8 cm, the dependence of both P_{out} and η on total current is presented in Fig. 3. About the output power, it is seen in Fig. 3 that P_{out} closely follows a linear increase with current before saturating at 320 kW for current levels above 230 A; the corresponding efficiency curve features a flat region of 14.5% efficiencies. Similar plots of P_{out} and η for R_I=0.9 cm are given in Fig. 4. In this case, while saturating at 670 kW for currents in excess of 525 A, the output power reaches the optimal value of 560 kW at 14.8% efficiency and 378 A current.

For the higher power case discussed above, the total time history of output power at z=5.0 cm is shown in Fig. 5. On steady state the constant-amplitude signal corresponds to the average power level of 560 kW. It is to be noted that the waveform amplitude is always positive, meaning that the output signal is a positive traveling wave. The frequency spectrum of the steady state electric field at the point z=5.0cm, r=1.0cm in the output guide is shown in Fig. 6, with a sharp spectrum centered at 6.67GHz, very close to the cold cavity eigenfrequency of 6.68 GHz.

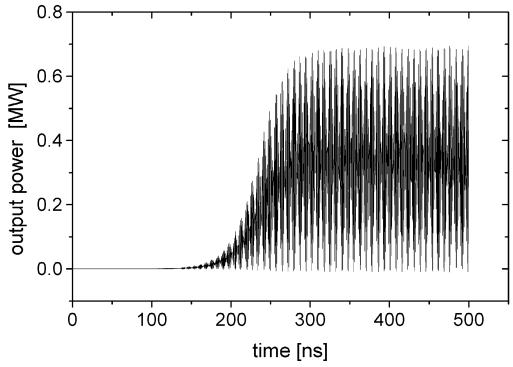

Fig. 5. *Total time history of RF output power at section z=5.0cm of the output guide.*

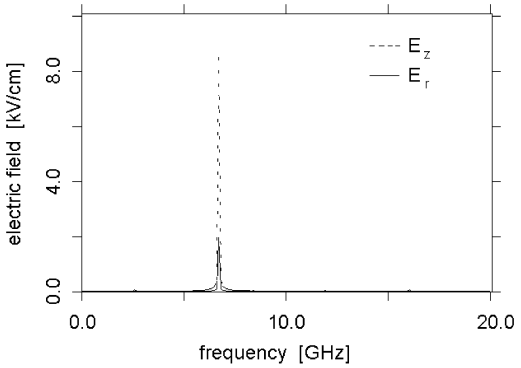

Fig. 6. *Frequency spectrum of electric field at r=1.0cm, z =5.0cm.*

5. Conclusions

A triple-beam TM_{040} monotron oscillator has been presented for which a 2½-D particle-in-cell simulation has indicated output powers in excess of 500 kW at 6.7GHz. The system includes a simple structure where the elementary functions of electron bunching and energy transfer to the RF field are performed in a single circular cylindrical cavity, which makes the monotron a compact, lightweight device. The cavity geometry (radius 8.42 cm, length 1.0 cm) and operating beam energy (10 keV) have been determined on the basis of a one-dimensional analysis, upon neglecting space-charge forces, that predicts a conversion efficiency of about 15.5%. The system has mechanical simplicity, and circular symmetry, for easy machining and assembly as well as a solid anode block for improved cooling and thermal management in long pulse operation. Such characteristics make the device practical from the viewpoint of cost and flexibility, allowing simple procedures for scaling power and frequency.

References

[1] C. K. Birdsall, and W. B. Bridges, *Electron Dynamics of Diode Regions*, New York: Academic Press, 1966, sec. 1.06.

[2] J. J. Müller and E. Rostas, "Un generateur a temps de transit utilisant un seul resonateur de volume", *Helvet. Phys. Acta*, vol. 13, pp. 435-450, Oct. 1940.

[3] J. J. Barroso, and K. G. Kostov "A 5.7GHz, 100 kW microwave source based on the monotron concept", *IEEE Trans. Plasma Science*, vol. 27, pp. 580-586, April 1999.

[4] J. J. Barroso, "Design facts in the axial monotron", *IEEE Trans. Plasma Science*, vol. 28, pp. 652-656, June 2000.

[5] V. P. Tarakanov, "User's Manual for Code KARAT", Berkeley Research Associates., Inc., Springfield, USA, 1994.

Present Status of ETE Diagnostics

L. A. Berni, M. Machida[1], M.J.R Monteiro[1], R. M. Oliveira , E. Del Bosco ,W. A. Vilela, M. Ueda, D. Cioban[1], A.M. Daltrini[1], R.M. Castro, J. G. Ferreira ,G. O. Ludwig
Instituto Nacional de Pesquisas Espaciais, Laboratório Associado de Plasma (INPE/LAP)
São José dos Campos, SP, Brasil, CEP 12201-970
[1] Universidade Estadual de Campinas, Instituto de Física "Gleb Wataghin" (UNICAMP/IFGW)
Campinas, SP, Brasil, CEP 13083-970

1. Introduction

The spherical tokamak ETE (**E**xperimento **T**okamak **E**sférico) [1] has started its operation at LAP/INPE. The ETE is a small aspect ratio tokamak (R/a = 1.5), with major radius R = 0.3 m and minor radius a = 0.2 m. In the first phase of operation the following macroscopic plasma parameters are expected: toroidal induction field of 0.4 T, ohmic current up to 220 kA, plasma pulse duration of 15 ms, density of about 5×10^{19} m^{-3} and temperature around 300 eV. A set of fundamental diagnostics is now being implemented comprising electromagnetic, Thomson scattering, mass spectrometer, fast visible spectroscopy and CCD camera. Other diagnostics as fast neutral lithium beam probe, CO_2 interferometer and soft X-ray tomographer are being developed.

2. Available diagnostics

Some of the electromagnetic diagnostics are already installed, including three Rogowski coils to measure the currents in the toroidal, vertical and ohmic circuits; one Rogowski coil placed inside the chamber for plasma current measurements and one outside the vessel to measure the induced current; twelve loop voltage coils (six around the vessel, five around the ohmic heating solenoid and one inside the chamber), and four magnetic probes inside the vessel to measure the vertical and radial fields. Figure 1 shows the signals of an initial ETE shot, with 11 kA in the toroidal magnetic coils, 4 kA in the ohmic coils and 2 kA in the equilibrium coils. The ETE vacuum vessel manufactured with Inconel has no electrical break in the toroidal direction. For the shot presented in figure 1, the induced current in the vessel reached 60 kA. For this shot a plasma current of about 8 kA was obtained with loop voltage of 15 V.

A high speed CCD camera with 1/500 to 1/20,000 frame speed and 30 to 500 FPS (upgradeable to 10,000 FPS) is being used. Since in the present condition the duration of the discharge is limited to 1.5 ms, just one frame per shot can be obtained. Figure 2 shows the upper part of the plasma cross-section taken with the CCD camera. The expected D-shaped cross section is clearly observed. A monochromator (1200 lines/mm, 12 Å/mm) coupled with a photomultiplier tube has been installed for ion temperature measurements by Doppler broadening. The $H_á$ behavior is being measured by a fixed slit (22 Å) monochromator with a photomultiplier tube. A photodiode is being used to measure the continuous emission (300 nm to 1100 nm). A mass spectrometer connected to the port of the vacuum system is used for measurements during vacuum chamber conditioning.

3. Diagnostics being installed

A 10J ruby laser Thomson scattering system (TS) [2] is being assembled (figure 3) to measure the plasma density and temperature profiles. A special collection lens allows to measure up to 22 spatial plasma points (with 15 mm spatial resolution) along the laser line and a five channel polychromator (that detects temperatures from 20 eV to 2 keV and densities greater than 10^{19} m^{-3}) will be used to measure the scattered light. A 1.3 m flight tube and a dump with special black anodized inserts were designed to prevent stray light effects.

A 10 keV Fast Neutral Lithium Beam probe (FNLB) [3] with current density up to 1 mA/cm^2 and life time of 400 min is being assembled for measurements of the boundary plasma density and its fluctuations. This plasma diagnostic method is adequate for use in fusion devices because it does not perturb the plasma and it provides data with high space and time resolution for the entire discharge lifetime. Figure 4 shows the schematic of the FNLB for the ETE tokamak. The ion beam is extracted from a heated (~ 1153^oC) glassy â-eucryptite [4] source and a set of three electrostatic lenses is used to extract, accelerate and collimate the beam that is neutralized by sodium vapor before entering the tokamak chamber. A flight tube with differential pumping prevents the plasma contamination. The lithium line profile will be measured at 90^o using a multichannel detection system composed of a spectrometer and photomultipliers, allowing simultaneous multipoint measurements.

4. Planned Diagnostics

One chord CO_2 (10.6μm) Michelson heterodyne interferometer modulated at 40 MHz has been designed to measure the line density. A HeNe laser (633 nm or 3.39 ìm) will be used to eliminate the effect of mechanical vibrations. The viability of a multipass interferometer to increase the wavelength shift is under consideration. Figure 5 shows this possibility, where two spherical mirrors can be set outside the vacuum vessel to reflect the CO_2 beam several times (22 passes in this case) before it leaves the plasma.

The application of a 64-channel photomultiplier for multipoint Thomson scattering is now under development [5]. Each channel of the detector has a 2.54mm × 2.54mm sensitive area, 5.0 ns response time, 10 stage dynodes with gain of $1x10^6$ at 1150 V, 270nm to 800nm spectral response, and 14% cross talk (measured) between channels. The detector is mounted on a SPEX spectrometer (11 Å/mm, f = 1 m) that allows temperature measurements up to 500 eV. Rayleigh and spectral calibration was performed in the plasma laboratory at UNICAMP. Figure 6 shows the multichannel detector intensity calibration.

5. Conclusion

Since ETE started operation in November 2000 the main efforts are concentrated on conditioning the vacuum vessel to achieve better plasma discharges and to install the basic diagnostics. The TS system should be operational in a two months period and nitrogen Rayleigh scattering will be used for density calibration. The FNLB should start probing the plasma by the middle of 2002. The design of the interferometer system (INPE/UNICAMP) is ready and it should be operational in two years from now. Multichannel detectors for the TS upgrade are being developed jointly with the UNICAMP plasma group.

6. References

[1] E. Del Bosco, et al.; Proc. IAEA Technical Committee Meeting on Spherical Tori, 26-28 October, 1998, Tokyo, p 239

[2] M. Bassan, et al.; Rev. Sci. Instrum. 68 (1), 718 (1997)

[3] R.M. Oliveira, W.A Vilela, M. Ueda; Proc. 14th IAEA on Research Using Small Fusion Devices, 25-27 Jun., 2001, SP, Brazil

[4] M. Ueda, R.R. Silva, R.M Oliveira, et al; J. Phys. D: Appl. Phys. 30 (1997), 2711-2716

[5] L. Erikson et al.; IEEE Trans. Nucl. Sci., 34, 344 (1987)

Acknowledgements. The authors thank FAPESP, FINEP and CNPq for financial support. Thanks also to Dr. Odim Mendes Jr. for loaning the CCD camera (FAPESP 1998/3860-9).

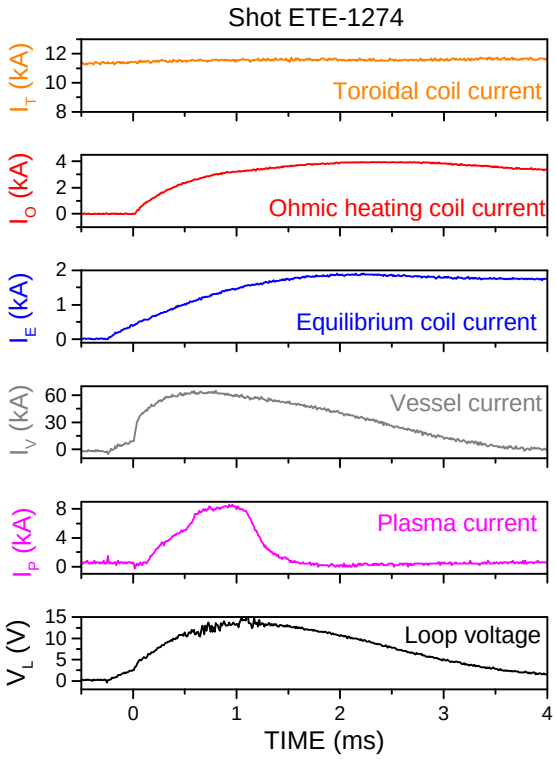

Figure 1. Rogowski and loop voltage signals

Figure 2. D-shaped plasma picture taken with the CCD camera

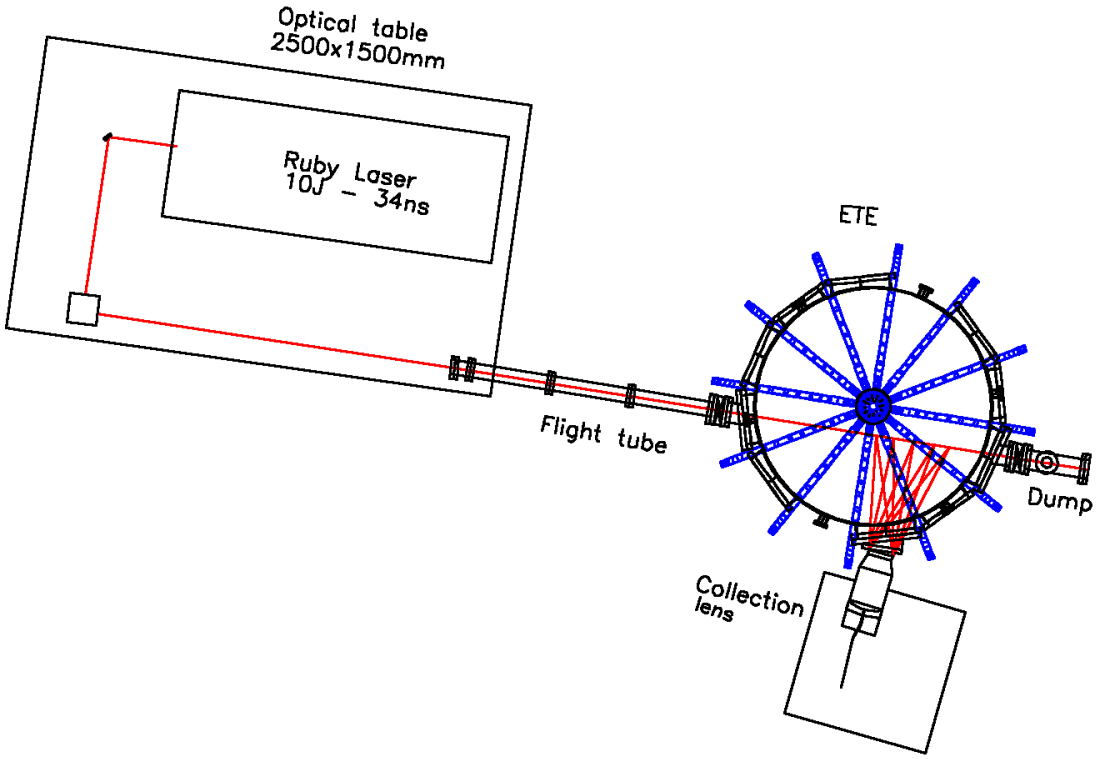

Figure 3. Thomson scattering system for the ETE tokamak

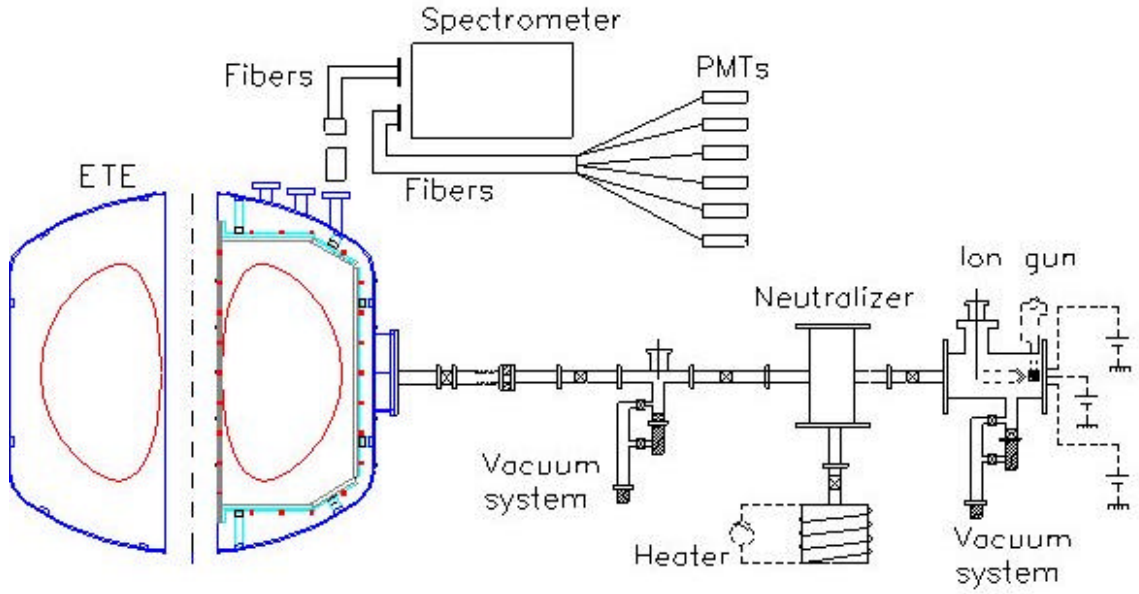

Figure 4. Lithium beam probe set up

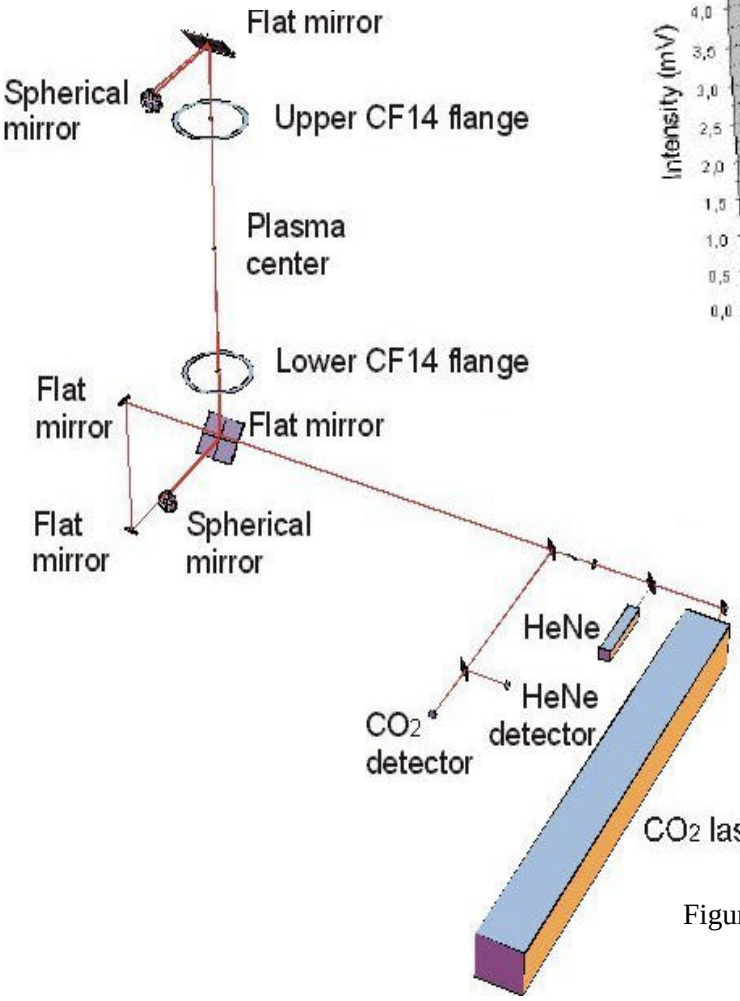

Figure 5. CO_2 multipass interferometer

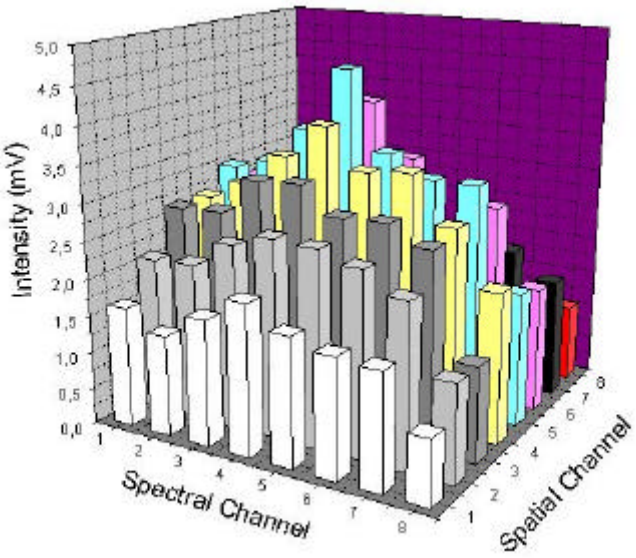

Figure 6. Multichannel detector intensity calibration

Overview of the ETE Spherical Tokamak Experiment

E. Del Bosco, J.G. Ferreira, L.A. Berni, R.M. Oliveira, G.O. Ludwig,
C.S. Shibata, H. Patire Jr., J.O. Rossi, W.A. Vilela, L.F.W. Barbosa

Instituto Nacional de Pesquisas Espaciais – INPE
Laboratório Associado de Plasma – LAP
São José dos Campos – CEP 12.227-010 – SP– Brazil

This paper gives an overview of the ETE spherical tokamak activities in course at LAP/INPE, emphasizing the measurements of stray fields in the plasma region, produced mainly by eddy currents in the vacuum vessel, as well as measurements of gas breakdown and first plasma formation.

Introduction

The ETE spherical tokamak is a small size machine with some innovative technological features making possible a compact design with good access for plasma diagnosis. The main objectives of ETE are the investigation of operating regimes and confinement properties with emphasis on the plasma edge physics, as well as diagnostics development in fusion-related plasmas with low aspect ratio configuration.

The construction of ETE was initiated in 1995 and the first tokamak plasma was obtained by 28 November 2000. Presently, the experiments are focused on plasma formation, wall conditioning and diagnostics implementation. ETE was designed to reach inductive toroidal plasma current up to 400kA for about 100ms of time duration and confined by an external toroidal magnetic field of less than 0.8T. With the present low energy configuration of the capacitor banks (toroidal field – TF: 128kJ, ohmic heating – OH: 160kJ/single swing and equilibrium field – EF: 76kJ), plasma current of the order of 30kA was expected with duration up to 5ms. These values were practically achieved, with a maximum plasma current of 34kA lasting 2.6ms and a typical current of 21kA lasting 3.3ms.

Stray magnetic fields play an important role during the gas breakdown and plasma formation. Measurements of these fields without plasma are presented. It is shown that even with a relatively high eddy current in the vacuum vessel a null in the magnetic field configuration is formed, allowing the plasma formation. Plasma equilibrium is already achieved as confirmed by a CCD picture of the plasma cross-section. Optimization of the operating parameters, wall conditioning and increase of the capacitor banks energy is under way in order to reach the design values.

Apparatus

The assembly of the machine was completed successfully with an overall precision of about 2mm according to a very strict design. The central stack (ℓ = 1.87m, d = 168.8mm), which is composed by the 12 internal TF coil legs and by a two layers (130 turn each) solenoid was the most challenging piece completely manufactured in our laboratory. Table 1 gives the main parameters of the coils after assembling and the maximum currents actually obtained.

Baking of the vacuum vessel is presently limited to about 75^{o} C due to the lack of a thermal isolation blanket. During glow discharge cleaning a variable butterfly-like valve placed in front of the turbo-drag pump controls the gas flow. Viton O'rings are still fitted in a few ports. The minimum base pressure already achieved is about 10^{-7} mbar. A stainless steel frame (with electric insulation breaks) is placed inside the vessel in one toroidal location, holding bars of high purity graphite used as limiters. This frame also protects the Rogowski

coil and a few magnetic pick-up coils. A total flux coil is also placed inside the vacuum vessel to measure the loop voltage at R = 0.443m.

Figure 1 presents the temporal current profiles of the three main coil circuits as well as the current induced in the vacuum vessel. The coil currents shown are the maximum obtained in the present configuration of the capacitor banks. The current rise in the TF coil is obtained by firing a fast bank (0.9kV) and the flat top (10ms) is maintained by firing three slow banks (90V each). The toroidal field at R = 0.3m is about 0.0078T/kA. The current waveform in the equilibrium coil is pre-programmed using one fast bank (2kV) and two slow banks (200V each). The maximum vertical field is about 35mT obtained when eddy currents in the vessel have already decayed. The current rise in the OH coil is produced by discharging a fast bank (4kV), which breaks down the gas insulation, and the plasma current is maintained by firing one slow bank (2kV). The maximum induced voltage at R_0 due to the OH coil is about 7.2V. This value can reach about 10V when the equilibrium field is also present.

Coil	R (mm)	Z (mm)	Turns	I (kA)
Solenoid	72.7	0	2×130	~ 4
Compensation 1	102	± 657	2×10	~ 4
Compensation 2	651	± 883	1×2	~ 4
Elongation	200	± 830	4×4	-
Equilibrium	700	± 422	4×4	~ 2
Toroidal	-	-	12 D-shaped in series	~ 11

Table 1. Parameters of the coils

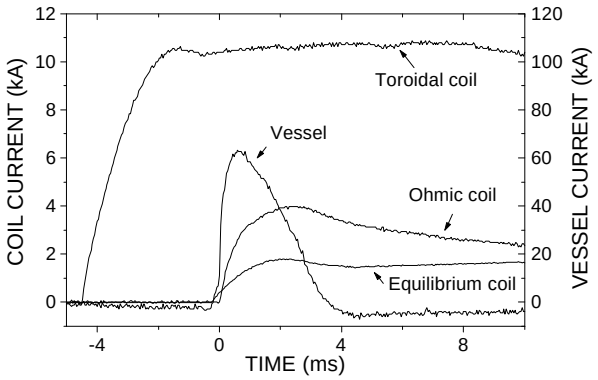

Figure 1. Waveforms of the currents in the coils and current induced in the vacuum vessel

Stray fields

Stray fields in the plasma region can be generated by several means: bad compensation of the solenoid, misalignment of poloidal coils, bending of TF coils, and induced currents. These fields are undesirable during plasma formation since they can prevent gas breakdown. Because the vacuum vessel of ETE has no electrical break in the toroidal direction relatively high values are expected for the current induced on its walls, notwithstanding the high electrical resistive Inconel alloy used in its manufacture. This current is in opposite direction relative to the currents in the coils, reaching its peak at the very beginning of the poloidal field bank discharges. Preliminary measurements of these stray fields were carried out and are presented in the following.

Figure 2 shows the radial profiles of the vertical magnetic field (B_z) due to the equilibrium (open squares), ohmic heating (open circles) and toroidal (open triangles) circuits as well as the total B_z produced by firing all banks together (solid squares and line). The fields were measured approximately at 0.2ms after triggering the OH bank, which corresponds roughly to the instant of breakdown. The values of the coil and vessel currents in that instant of time are also shown in the picture. It can be observed from figure 2 that the total B_z profile crosses the zero-axis at R ~ 0.45m. It is noteworthy to point out that the vertical equilibrium field (open squares) is not a stray field; on the contrary, its trigger time is experimentally adjusted in order to compensate for the stray fields creating the null point. Figure 3 shows the radial profile of the radial magnetic field, B_r, generated by the ohmic heating (solid circles) and equilibrium (open squares) circuits for the same conditions of figure 2.

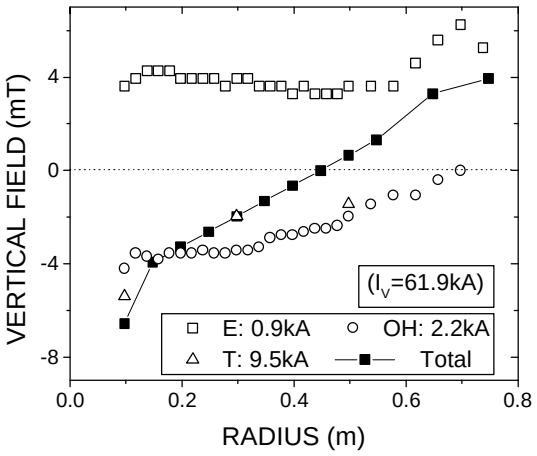

Figure 2. B_z radial profile due to ohmic heating, equilibrium and toroidal coil currents

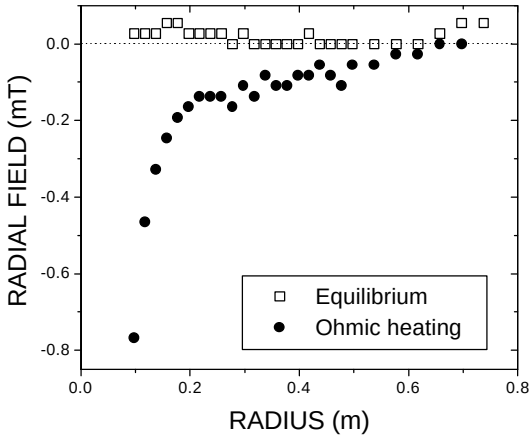

Figure 3. B_r radial profile due to ohmic heating and equilibrium coil currents

Figure 4 shows the radial profile of the vertical magnetic field, B_z, (solid squares) created by the OH coils alone when the value of the coil current reaches its maximum (3.9 kA). At this instant the induced current in the vessel is 19.5kA in the opposite direction. The dash-dotted line represents the calculated profile taking into account only the OH coils, while the dashed line is the profile computed modeling the vessel as 32 filaments. The solid line is the total calculated profile. The filaments and currents distribution in the vessel are being optimized considering measurements of the current taken in different parts of the vessel with the ports open, as well as the thickness of the wall around the poloidal plane. Figure 5 shows the B_z radial profile for the equilibrium coils at two different instants of the same shot: the open squares represent the instant when the induced current in the vessel is high (20.9kA) while the solid squares are taken when the induced current has already decayed to zero. In both profiles the current in the coils is about the same, 1.8kA. The lines in figure 5 are calculated profiles; the dashed one is for I_{vessel} = 20.9kA while the solid one is for I_{vessel} = 0.

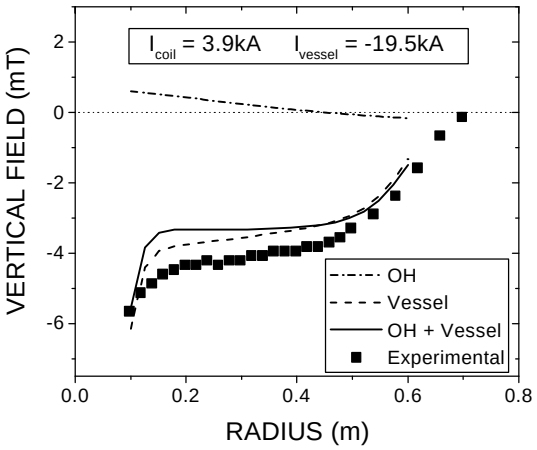

Figure 4. B_z radial profile due to the ohmic heating coil current and calculated profiles

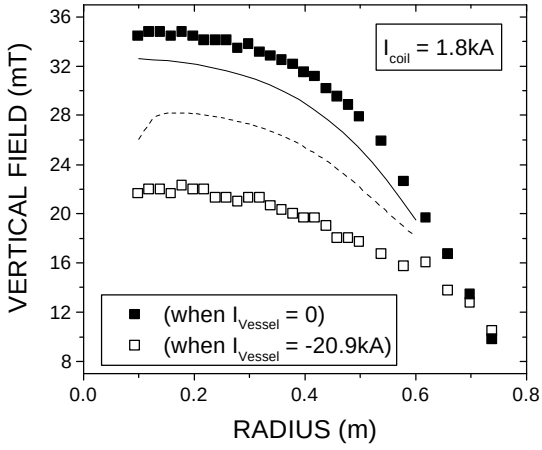

Figure 5. B_z radial profile due to the equilibrium coil current and calculated profiles

Breakdown

A preliminary study of the gas breakdown in ETE was carried out. The characteristic breakdown curve, electric field versus gas pressure, and the time lag versus gas pressure were measured for three different conditions: no pre-ionization, UV lamp, and hot filament pre-ionization (4A×47V, 75V polarization). Figure 6 shows the E×P curves and figure 7 shows the τ_{lag}×P curves. The electric field was measured with a total flux coil placed inside the vessel. The time lag was defined as the time interval between the application of the OH bank and the beginning of the plasma current. Hydrogen gas was continuously supplied and the pressure was measured with an ion gauge. The beneficial effect of pre-ionization is clearly observed in these figures. Electric field values as low as 2V/m are enough for breakdown.

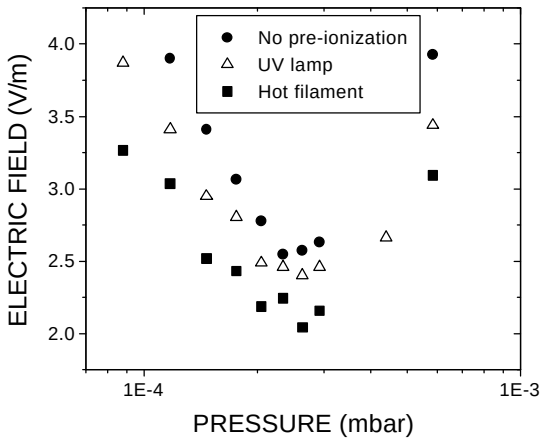

Figure 6. E×P curves for H_2 breakdown in ETE.

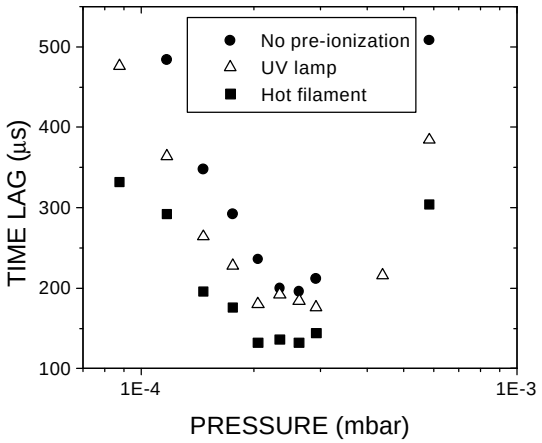

Figure 7. Time lag for gas breakdown in ETE

Equilibrium

The equilibrium of the plasma current in ETE was confirmed using a high-speed CCD camera. Figure 8 shows the picture of the plasma cross-section taken during shot 1404, when the plasma current was about 8kA. The D-shaped cross section of the plasma is clearly observed.

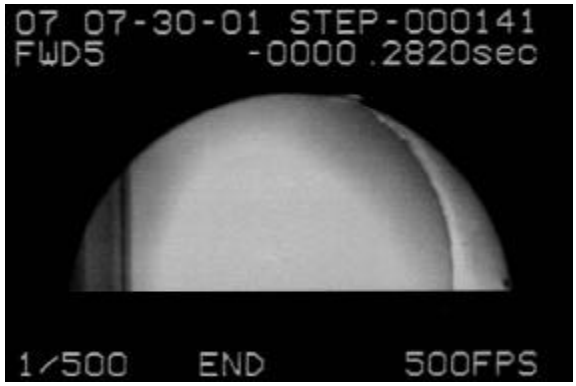

Figure 8. CCD photo of the plasma cross section

Conclusions

The ETE spherical tokamak was successfully assembled. The first plasma was obtained by the end of 2000. The eddy current in the vacuum vessel is being modeled in order to optimize the gas breakdown and plasma formation. By properly setting the time delay between the ohmic heating and vertical banks, the gas breakdown is easily obtained even without pre-ionization. Plasma equilibrium is being achieved. Wall conditioning (DC glow and baking) is now under way in order to increase the plasma current as well as the discharge duration. Capacitor banks have to be completed in order to reach the design values.

Acknowledgments: The authors give thanks to FAPESP, Finep, CNPq and IAEA for financial support and Dr. O. Mendes (CEA/INPE) for loaning the fast CCD camera.

RADIO FREQUENCY WAVE DISSIPATION BY ELECTRON LANDAU DAMPING IN ELONGATED SPHERICAL TOKAMAKS

N.I. Grishanov[1], C.A. de Azevedo[2], G.O. Ludwig[3], J.P. Neto[1,2]

[1]*Laboratório Nacional de Computação Científica, 25651-070 Petrópolis, Brazil*
[2]*Universidade do Estado do Rio de Janeiro, 20550-013 Rio de Janeiro, Brazil*
[3]*Instituto Nacional de Pesquisas Espaciais, 12221-010 São José dos Campos, Brazil*

Spherical Tokamaks (or Low Aspect Ratio Tokamaks) represent a promising alternative route to magnetic thermonuclear fusion. In order to achieve fusion conditions in these devices additional plasma heating must be employed. Effective schemes of heating and current drive in tokamak plasmas can be realized using radio frequency waves. As is well known, the kinetic wave theory of any toroidal plasma should be based on the solution of the Vlasov-Maxwell's equations. However, this problem is not simple even in the scope of linear theory since to solve the wave (or Maxwell's) equations it is necessary to use the correct dielectric (or wave conductivity) tensor valid in the given frequency range for the realistic two- or three-dimensional plasma model. In this paper, the longitudinal permittivity elements are derived for radio frequency waves in a two-dimensional axisymmetric tokamak with elliptic magnetic surfaces, for arbitrary elongation and arbitrary aspect ratio. A high-temperature collisionless plasma model is considered. The drift-kinetic equation is solved separately for untrapped and usual *t*-trapped particles as a boundary-value problem, in the case when the so-called [6] *d*-trapped particles are absent in the plasma, using an approach developed [7] for Low Aspect Ratio Tokamak (LART) with circular magnetic surfaces. To describe an elongated tokamak we use the variables (r,θ') instead of quasi-toroidal co-ordinates (ρ,θ) [7]:

$$r = \rho\sqrt{\frac{a^2}{b^2}\sin^2\theta + \cos^2\theta}\,, \qquad \theta' = 2\arctan\left[\sqrt{\frac{1-\varepsilon}{1+\varepsilon}}\tan\left(\frac{1}{2}\arctan\left(\frac{a}{b}\tan\theta\right)\right)\right], \tag{1}$$

transforming the initial elliptic cross-sections of the magnetic surfaces to circles with the maximum radius a of the external magnetic surface. In the (r,θ')-coordinates, the magnetic field lines become "straight", and the modulus of the equilibrium magnetic field, $H=|\mathbf{H}|$, is

$$H(r,\theta') = \sqrt{H_{\phi 0}^2 + H_{\theta 0}^2}\, g(r,\theta')\,, \quad g(r,\theta') = \frac{\sqrt{(1-\varepsilon\cos\theta')^2 + \lambda(\varepsilon-\cos\theta')^2}}{1-\varepsilon^2}\,, \tag{2}$$

where $\varepsilon = \dfrac{r}{R}$, $\lambda = h_\theta^2\left(\dfrac{b^2}{a^2}-1\right)$, $h_\phi = \dfrac{H_{\phi 0}}{\sqrt{H_{\phi 0}^2 + H_{\theta 0}^2}}$, $h_\theta = \dfrac{H_{\theta 0}}{\sqrt{H_{\phi 0}^2 + H_{\theta 0}^2}}$,

$H_{\varphi 0}(r)$ and $H_{\theta 0}(r)$ are the toroidal and poloidal projections of **H** for a given magnetic surface at the points $\theta = \pm\pi/2$; R is the major tokamak radius; b and a are the major and minor semiaxes of the elliptical cross-section of the external magnetic surface. In this model, all magnetic surfaces are similar to each other with the same elongation equal to b/a.

To solve the drift-kinetic equation for plasma particles we use the standard method of switching to new variables associated with conservation integrals of energy, $v_\parallel^2 + v_\perp^2 = const$, and magnetic moment, $v_\perp^2 / 2H = const$. Introducing the variables v (particle energy) and μ (nondimensional magnetic moment) in velocity space instead of $v_\parallel$ and $v_\perp$:

$$v^2 = v_\parallel^2 + v_\perp^2\,, \qquad \mu = \frac{v_\perp^2}{v_\parallel^2 + v_\perp^2}\frac{\sqrt{H_{\phi 0}^2 + H_{\theta 0}^2}}{H(r,\theta')}\,, \tag{3}$$

the perturbed distribution function of plasma particles (any kind of ions and electrons) can be found as

$$f(t,r,\theta',\phi,v_{\|},v_{\perp}) = \sum_{s=\pm 1} f_s(r,\theta',v,\mu)\exp(-i\omega t + in\phi),$$

where we have taken into account that the problem is uniform in both time t and toroidal angle ϕ. In zero order over the magnetization parameters (i.e., neglecting finite Larmor radius effects), the linearized drift-kinetic equation for harmonics f_s can be written as

$$\frac{(1-\varepsilon\cos\theta')^2}{(1-\varepsilon^2)^{1.5}}\frac{\sqrt{1-\mu\cdot g(r,\theta')}}{g(r,\theta')}\left(\frac{\partial f_s}{\partial\theta'}+inqf_s\right)-i\frac{sr\omega}{h_\theta v}f_s = 2\frac{erE_{\|}F}{Mh_\theta v_T^2}\sqrt{1-\mu\cdot g(r,\theta')}, \qquad (4)$$

where $$F=\frac{N}{\pi^{1.5}v_T^3}\exp\left(-\frac{v^2}{v_T^2}\right), \qquad v_T^2=\frac{2T}{M}, \qquad g=\frac{\varepsilon\cdot h_\phi}{h_\theta\sqrt{1-\varepsilon^2}},$$

$E_{\|}=\mathbf{E}\cdot\mathbf{h}$ is the parallel (to **H**) electric field component; the steady-state distribution function F is given as a Maxwellian with the particle density N, temperature T, charge e and mass M. The index of particles species (ions and electrons) is omitted in Eqs. (4). By the indexes $s=\pm 1$ for f_s, we distinguish the perturbed distribution functions with positive and negative values of the parallel velocity $v_{\|}=sv\sqrt{1-\mu\cdot g(r,\theta')}$ relative to **H**.

Thus, the initial drift-kinetic equation is reduced to a first order differential equation with respect to the poloidal angle θ', where the variables r, v, μ (as well as R, a, b, q, N, T) appear as parameters. After solving Eq. (4), the longitudinal (parallel to **H**) component of the current density $j_{\|}=\mathbf{j}\cdot\mathbf{h}$ can be expressed as

$$j_{\|}(r,\theta') = \pi e g(r,\theta')\sum_{s}^{\pm 1} s\int_0^{\infty} v^3\int_0^{1/g(r,\theta')} f_s(r,\theta',v,\mu)\,d\mu\,dv \ . \qquad (5)$$

Depending on μ and θ' the phase space of plasma particles must be split in the phase space of untrapped, t-trapped and d-trapped particles according to the following inequalities:

$$0\le\mu\le\mu_u \qquad -\pi\le\theta'\le\pi \qquad \text{- for untrapped particles} \qquad (6)$$

$$\mu_u\le\mu\le\mu_t \qquad -\theta_t\le\theta'\le\theta_t \qquad \text{- for } t\text{-trapped particles} \qquad (7)$$

$$\mu_t\le\mu\le\mu_d \qquad -\theta_t\le\theta'\le-\theta_d \qquad \text{- for } d\text{-trapped particles} \qquad (8)$$

$$\mu_t\le\mu\le\mu_d \qquad \theta_d\le\theta'\le\theta_t \qquad \text{- for } d\text{-trapped particles} \qquad (9)$$

where [analyzing the condition $v_{\|}(\mu,\theta')=0$]

$$\mu_u=\frac{1-\varepsilon}{\sqrt{1+\lambda}}, \qquad \mu_t=\frac{1+\varepsilon}{\sqrt{1+\lambda}}, \qquad \mu_d=\varepsilon\frac{1+\lambda}{\lambda+\varepsilon^2},$$

and the reflection points $\pm\theta_t$ and $\pm\theta_d$ for t- and d-trapped particles are, respectively,

$$\pm\theta_t=\pm\arccos\left\{\frac{\varepsilon(1+\lambda)}{\lambda+\varepsilon^2}-\sqrt{\frac{\varepsilon^2(1+\lambda)^2}{(\lambda+\varepsilon^2)^2}-\frac{1}{\lambda+\varepsilon^2}\left[1+\varepsilon^2\lambda-\left(\frac{1-\varepsilon^2}{\mu}\right)^2\right]}\right\}. \qquad (10)$$

$$\pm\theta_d=\pm\arccos\left\{\frac{\varepsilon(1+\lambda)}{\lambda+\varepsilon^2}+\sqrt{\frac{\varepsilon^2(1+\lambda)^2}{(\lambda+\varepsilon^2)^2}-\frac{1}{\lambda+\varepsilon^2}\left[1+\varepsilon^2\lambda-\left(\frac{1-\varepsilon^2}{\mu}\right)^2\right]}\right\} \qquad (11)$$

Now, we solve Eq. (4) for untrapped and usual t-trapped particles only, under the condition when the d-particles are absent, i.e., considering the LART magnetic field configuration as a system with one minimum of $\mathbf{H}(r,\theta')$. In this case, the criterion [6] of d-particle existence, $\varepsilon<\lambda$ or $b/a>\sqrt{1+\varepsilon+q^2(1-\varepsilon^2)/\varepsilon}$, cannot be satisfied.

The solution of Eq. (4) must be found for the specific boundary conditions of the trapped and untrapped particles. For untrapped particles we use the periodicity of f_s over θ'. Whereas, the boundary condition for the t-trapped particles is the continuity of f_s at the corresponding stop-points, Eq. (10). As a result, we seek the perturbed distribution functions of untrapped, f_s^u, and t-trapped, f_s^t, particles as

$$f_s^u = \sum_p^{\pm\infty} f_{s,p}^u \exp\left[i2\pi(p+nq)\frac{\tau(\theta')}{T_u} - inq\theta' \right], \quad f_s^t = \sum_p^{\mp\infty} f_{s,p}^t \exp\left[i2\pi p\frac{\tau(\theta')}{T_t} - inq\theta' \right] \qquad (12)$$

where p is the number of resonance bounces,

$$\tau(\theta') = \int_0^{\theta'} \frac{(1-\varepsilon^2)\cdot g(r,\eta)\cdot d\eta}{(1-\varepsilon\cos\eta)^2\sqrt{1-\mu g(r,\eta)}} \qquad (13)$$

is the new time-like variable (instead of θ') describing the bounce-periodic motion of untrapped and t-trapped particles along the magnetic field line with the corresponding periods $T_u = 2\tau(\pi)$ and $T_t = 4\tau(\theta_t)$. The Fourier harmonics $f_{s,p}^u$ and $f_{s,p}^t$ for untrapped and t-trapped particles can be readily derived after the corresponding bounce averaging.

To evaluate the dielectric tensor elements we use the Fourier expansions of the current density and electric field over the poloidal angle θ':

$$\frac{j_\parallel(\theta')}{(1-\varepsilon^2)g(r,\theta')} = \sum_m^{\pm\infty} j_\parallel^m \exp(im\theta'), \quad E_\parallel(\theta')\frac{(1-\varepsilon^2)g(r,\theta')}{(1-\varepsilon\cos\theta')^2} = \sum_{m'}^{\pm\infty} E_\parallel^{m'} \exp(im'\theta') \qquad (14)$$

As a result, the whole spectrum of electric field, $E_\parallel^{m'}$, is present in the given m-th harmonic $j_\parallel^m$ of the current density:

$$\frac{4\pi i}{\omega} j_\parallel^m = \sum_{m'}^{\pm\infty} \varepsilon_\parallel^{m,m'} E_\parallel^{m'} = \sum_{m'}^{\pm\infty} (\varepsilon_{\parallel,u}^{m,m'} + \varepsilon_{\parallel,t}^{m,m'}) E_\parallel^{m'} \ , \qquad (15)$$

where $\varepsilon_{\parallel,u}^{m,m'}$ and $\varepsilon_{\parallel,t}^{m,m'}$ are the separate contributions of untrapped and t-trapped particles, respectively, to the longitudinal (parallel) permittivity elements:

$$\varepsilon_{\parallel.u}^{m,m'} = \frac{\omega_p^2 r^2}{h_\theta^2 v_T^2 \pi^3} \sum_{p=-\infty}^{\infty} \int_0^{\mu_u} \frac{\tau(\pi) C_p^m C_p^{m'}}{(p+nq)^2} \left[1 + 2u_p^2 + 2i\sqrt{\pi} u_p^3 W(u_p) \right] d\mu \,, \qquad (16)$$

$$\varepsilon_{\parallel.t}^{m,m'} = \frac{2\omega_p^2 r^2}{h_\theta^2 v_T^2 \pi^3} \sum_{p=1}^{\infty} \int_0^{\mu_t} \frac{\tau(\theta_t)}{p^2} D_p^m D_p^{m'} \left[1 + 2v_p^2 + 2i\sqrt{\pi} v_p^3 W(v_p) \right] d\mu \,. \qquad (17)$$

Here we have used the following definitions

$$\omega_p^2 = \frac{4\pi N e^2}{M}, \qquad u_p = \frac{r\omega\sqrt{1-\varepsilon^2}\tau(\pi)}{h_\theta \mid p+nq \mid v_T \pi}, \qquad v_p = 2\frac{r\omega\sqrt{1-\varepsilon^2}\tau(\theta_t)}{h_\theta p v_T \pi},$$

$$C_p^m = \int_0^{\pi} \cos\left[(m+nq)\eta - (p+nq)\pi\frac{\tau(\eta)}{\tau(\pi)} \right] d\eta \,, \qquad W(z) = e^{-z^2}\left(1 + \frac{2i}{\sqrt{\pi}} \int_0^z e^{t^2} dt \right),$$

$$D_p^m = \int_0^{\theta_t} \cos\left[(m+nq)\eta - p\frac{\pi\tau(\eta)}{2\tau(\theta_t)} \right] d\eta + (-1)^{p-1} \int_0^{\theta_t} \cos\left[(m+nq)\eta + p\frac{\pi\tau(\eta)}{2\tau(\theta_t)} \right] d\eta \,.$$

It should be noted that Eqs. (16, 17) describe the contribution of any kind of untrapped and trapped particles to the dielectric elements. The corresponding expressions for plasma electrons and ions can be obtained from (16, 17) replacing T, N, M, e by the electron T_e, N_e, m_e, e_e and ion Ti, N_i, M_i, e_i parameters, respectively. To obtain the total expressions of the permittivity elements, as usual, it is necessary to carry out the summation over all species of plasma particles.

One of the main mechanisms of radio frequency plasma heating is the electron Landau damping of waves due to the Cherenkov resonance interaction of $E_\parallel$ with the trapped and untrapped electrons. Cherenkov resonance conditions are different for trapped and untrapped particles in the LART plasmas and have nothing in common with the wave-particle resonance condition in cylindrical magnetized plasmas. Another important feature of tokamak plasmas is the contributions of all $E_\parallel^{m'}$-harmonics to the given $j_\parallel^m$-harmonic, Eq. (15). As a result, after averaging in time and poloidal angle, the wave power absorbed, $P = \mathrm{Re}(E_\parallel \cdot j_\parallel^*)$, due to trapped and untrapped electrons can be estimated by the expression

$$P = \frac{\omega}{8\pi} \sum_{m}^{\pm\infty} \sum_{m'}^{\pm\infty} \left(\mathrm{Im}\,\varepsilon_{\parallel,u}^{m,m'} + \mathrm{Im}\,\varepsilon_{\parallel,t}^{m,m'} \right) \left(\mathrm{Re}\,E_\parallel^m\ \mathrm{Re}\,E_\parallel^{m'} + \mathrm{Im}\,E_\parallel^m\ \mathrm{Im}\,E_\parallel^{m'} \right), \qquad (18)$$

where $\mathrm{Im}\,\varepsilon_{\parallel,u}^{m,m'}$ and $\mathrm{Im}\,\varepsilon_{\parallel,t}^{m,m'}$ are the contributions of untrapped and *t*-trapped electrons to the imaginary part of the longitudinal permittivity elements: $\mathrm{Im}\,\varepsilon_\parallel^{m,m'} = \mathrm{Im}\,\varepsilon_{\parallel,u}^{m,m'} + \mathrm{Im}\,\varepsilon_{\parallel,t}^{m,m'}$. In the simplest case of Toroidicity-induced Alfvén Eigenmodes (TAEs) [8], describing the coupling of only two harmonics with m_o and m_o-1, the width m_o, m_o-1 should also be accounted in Eq. (15) to estimate the TAEs absorption by the trapped and untrapped electrons. As a result, the dissipated power of TAEs by electron Landau damping is

$$P = \frac{\omega}{8\pi} \sum_{m=m_o-1}^{m_o} \mathrm{Im}\,\varepsilon_\parallel^{m,m'} \mid E_\parallel^m \mid^2 + \frac{\omega}{4\pi} \mathrm{Im}\,\varepsilon_\parallel^{m_o,m_o-1} \left(\mathrm{Re}\,E_\parallel^{m_o}\ \mathrm{Re}\,E_\parallel^{m_o-1} + \mathrm{Im}\,E_\parallel^{m_o}\ \mathrm{Im}\,E_\parallel^{m_o-1} \right) \qquad (19)$$

where $\mid E_\parallel^m \mid^2 = (\mathrm{Re}\,E_\parallel^m)^2 + (\mathrm{Im}\,E_\parallel^m)^2$. Note that the non-diagonal elements $\varepsilon_\parallel^{m,m'} \mid_{m \neq m'}$ are characteristic only of toroidal plasmas. For the one-mode (cylindrical) approximation, when $m=m'=m_o$, the non-diagonal elements vanish, i.e., $\mathrm{Im}\,\varepsilon_\parallel^{m,m'} \mid_{m \neq m'} = 0$, and Eqs. (18, 19) reduce to the well-known expression

$$P = \frac{\omega}{8\pi} \mathrm{Im}\,\varepsilon_\parallel^{m,m} \mid E_\parallel^m \mid^2 .$$

The longitudinal permittivity elements evaluated in this paper are suitable for both large and low aspect ratio tokamaks with elliptic magnetic surfaces and valid in a wide range of wave frequencies, mode numbers, and plasma parameters. The expressions (16, 17) have a natural limit to the corresponding results [7] for LART plasmas with circular magnetic surfaces, if b=*a* and $\lambda \to 0$. Since the drift kinetic equation is solved as a boundary-value problem, the longitudinal permittivity elements (16, 17) are suitable for studying wave processes with a regular frequency, such as wave propagation and dissipation during plasma heating and current drive generation, with wave frequency given, e.g., by the antenna-generator system.

References

[1] Y-K.M. Peng, D.J. Strickler, Nuclear *Fusion*, **26** 769, 1986.
[2] D.C. Robinson, Fusion *Energy and Plasma Physics*, World Scientific Press, 601, 1987.
[3] A. Sykes *et al, Plasma Phys. Control. Fusion*, **39** 247, 1997.
[4] A. Sykes and *MAST team*, X Int. Congress Plasma Phys. & 42 Annual Meeting of the DPP-APS, 23-27 October 2000, Quebec, Canada, paper GI1-2.
[5] S.M. Kaye and *NSTX Research Team*, *Ibiden*, paper GI1-3.
[6] N.I. Grishanov, C.A. Azevedo, A.S. Assis, *Plasma Phys.Control. Fusion*, **41** 645, 1999.
[7] N.I. Grishanov, C.A. Azevedo, J.P. Neto, *Plasma Phys. Control. Fusion*, August, 2001.
[8] C.Z. Cheng, M.S. Chance, Phys. *Fluids*, 29 3695, 1986.